Development of a DXA–Based Patient–Specific Finite Element Model for Assessing Osteoporotic Fracture Risk

by

Zannatul Ferdous

A Thesis submitted to the Faculty of Graduate Studies of

The University of Manitoba

in partial fulfilment of the requirements of the degree of

MASTER OF SCIENCE

Department of Mechanical & Manufacturing Engineering

University of Manitoba

Winnipeg

Abstract

In this thesis, a 2D finite element model was developed from patient's DXA image to evaluate the osteoporotic fracture risk. The loading configuration was designed to simulate a fall onto the greater trochanter. Bone inhomogeneous mechanical properties (Young's modulus) assigned to the FE model were correlated to bone mineral density captured in DXA image using empirical functions. The in-house developed MATLAB codes were implemented and used to investigate the effect of different factors like bone mineral density, femoral neck length, neck diameter, neck angle and patient's body weight. The 2D FE model constructed from DXA image was able to determine the factors which affect fracture risk to a greater extent based on the location of femur. The model developed here can be considered as a first attempt for investigating the effects of different parameter on FRI using patient specific 2D FE method.

Acknowledgments

I would like to express my immense appreciation to my supervisor, Professor Yunhua Luo, for his support and insightful guidance in my research, and also for his generous help in the non-academic area which greatly encouraged me during my study in Canada. I would also like to express my gratitude to my co-supervisor, Professor Qiang (Chong) Zhang for his help in preparation of my technical papers. My sincere thanks also go to Professor U. P. Wyss and Professor Q. Peng for their advice and help on my course studies.

The research reported in this thesis has been partially supported by the Manitoba Health Research Council (MHRC) which is gratefully acknowledged. I also gratefully acknowledge the Manitoba Bone Mineral Density Program and the St. Boniface Hospital for providing the clinical cohorts for conducting the study.

I would also like to thank Zhaoyang Liang, Pei Zhang and Chan Nan Wu for all the academic discussion and happy time working with them. I am grateful to all the friends I have made in Winnipeg for bringing me so many joyful moments and encouragement.

Finally, I would like to express my deep love and appreciation to my parents, husband, brother, sister, brother-in-law, sister-in-law, for their consistent and unconditional love and support.

Dedication

To my parents

Contents

List of Tables

List of Figures

List of Copyrighted Materials

Figure 2-1 was cited from "R. Ruimerman, 'Modeling and remodeling in bone tissue,' Ph.D. dissertation, Technische Universiteit Eindhoven, 2005". The permission was obtained on May 10, 2012.

Figure 2-2: Permission of using that figure was obtained on May 01, 2012.

Available from URL: http://courses.washington.edu/conj/bess/bone/bone2.html

Figure 2-3: Permission of using that figure was obtained on May 04, 2012.

Source of the figure: "informedhealthonline.org".

Available from URL: http://www.informedhealthonline.org/fact-sheet-preventing-osteoporosis.423.en.html

Figure 3-2: Permission of using that figure was obtained on May 04, 2012.

Source of the figure: "Capital Imaging Associates".

Available from URL: http://www.capitalimagingassoc.com/dxa.html

Figure 3-3 was cited from "G. M. Kiebzak, K. G. Faulkner, W. Wacker, R. Hamdy, E. Seier, and N. B. Watts, "Effect of precision error on t-scores and the diagnostic classification of bone status," *Journal of Clinical Densitometry*, vol. 10, pp. 239–243, 2007". Copyright was obtained on May 03, 2012.

List of Abbreviations

Areal Bone Mineral Density	aBMD
Bone Mineral content	BMC
Bone Mineral Density	BMD
Computed Tomography	CT
Dual Energy X-ray Absorptiometry	DXA
Finite Element Analysis	FEA
Finite Element Method	FEM
Fracture Risk Index	FRI
Hip Structure Analysis	HSA
Hounsfield Unit	HU
Neck Diameter	ND
Neck Length	NL
Region of Interest	ROI
Standard Deviation	SD
Total Length	TL
Two Dimensional	2D
Three Dimensional	3D
Volumetric Bone Mineral Density	vBMD
World Health Organization	WHO

List of Symbols

Total Area of region	A
Area of an element	A_e
Deformation Matrix	B
Material Property Matrix	D
Young's modulus	E
Global Stiffness Matrix	K
Element Stiffness Matrix	$k^{(e)}$
Shape Function Matrix	$N^{(e)}$
Coefficient of Determination	R^2
Coefficient of Correlation	r
Nodal Displacement	$U^{(e)}$
Yield Strength	σ_Y
Nodal Stress Vector	σ
Nodal Stress at *x*-direction	σ_x
Nodal Stress at *y*-direction	σ_y
Nodal Stress at *xy*-plane	τ_{xy}
Nodal Strain Matrix	ε
Nodal Strain at *x*-direction	ε_x
Nodal Strain at *y*-direction	ε_y
Nodal Strain at *xy*-plane	γ_{xy}
Probability of statistical significance	p

Chapter 1

Introduction

Hip fractures are the most serious consequences of osteoporosis [1, 2] and a major cause of suffering, disability and death in older women and men. The morbidity and mortality attributable to osteoporosis in elderly people is mainly caused by hip fractures [3, 4, 5]. On one hand, it increases the mortality and morbidity in older men and women; on the other hand, it is a substantial source of health care expenditure. In the United States alone, over 2 million osteoporotic fractures occurred in 2005 at a cost of $17 billion, and 72% of this total cost are accounted for hip fracture which is only 14% of the total incident fractures [6]. To recognize osteoporosis as health priority, October 20th was designated as "World Osteoporosis Day", with a call for health officials and researchers around the world.

Current available methods for *in-vivo* osteoporosis risk assessment are mainly based on statistical models and bone mineral density (BMD) measured by medical imaging modalities [7]. Femur DXA is primarily used for the evaluation of fracture risk as it is designated as a reference standard by the World Health Organization (WHO). Statistical models based on BMD derived from DXAs are effective in studying trends in osteoporosis and

correlations with fracture in large populations [8]. In these statistical analyses, T-score and Z-score are generally calculated where T-score shows the amount of bone of a patient has, compared to a young adult at peak bone mass and Z-score reflects the amount of bone that a person has, compared to other people in the person's age group and of the same ethnicity and gender [9].

One of the most important deficiencies of the statistical approach is that- it is only suitable on averaging over a group of people rather than individual analysis. DXA can merely provide the indication of relative risk but unable to predict the fracture risk. Moreover the measurement can be affected by the size of the patients or other factors extraneous to bone. In addition, the clinical consequences of osteoporosis are fragility fractures, the causation of which are multifactorial and include factors related to falls as well as additional skeletal components not captured by BMD (i.e. the micro architecture of bone). To date, it has become an urgent need for a more accurate method for the assessment of osteoporotic fracture risk.

At the same time, the accuracy in predicting individual fractures using only BMD is limited; most osteoporotic fractures occur with BMD measurements that are above the conventional osteoporotic threshold [8, 10, 11]. Bone tissue stress and strength contribute to fracture risk [12]. Furthermore, the material properties, mass and the spatial distribution of that mass (architecture and geometry) and the deforming force determine the mechanical effectiveness of any solid body [13, 14, 15]. Again the distribution of load throughout the bone is strongly influenced by the bone geometry [16].

The limitations of current statistical methods makes image-based finite element modeling attractive as one of the potential tools for investigating the factors affecting osteoporotic

fracture and treatment effectiveness. The information extracted from DXA can be implemented efficiently as measurements have already successfully validated in cadaveric testing. Medical image based finite element modeling is also considered as a very propitious technique for assessment of *in- vivo* bone strength. However, its usefulness in discriminating fracture risk has not yet been established due to a number of unresolved issues [17, 18]. Currently available DXA-based FE tools are developed using over-simplified engineering structural models [12, 19, 20]. A more advanced finite element modeling procedure is proposed and validated in this thesis which aims to assess osteoporotic fracture risk in individual patients.

The aim and objective of this thesis is to develop a two dimensional finite element model and investigate the influence of bone mechanical properties as well as structural properties on osteoporotic fracture risk based on a DXA image. Investigating fracture risk at three pre-defined clinically critical locations-i.e. at the femoral neck, the intertrochanter and the subtrochanter, is another important objective of this current research. Though the developed model has limitations, it may be considered as a first attempt for investigating the effects of different parameters on FRI using patient specific finite element method.

The thesis is organized as follows. In Chapter 2, bone structure and a brief introduction of osteoporosis will be presented. The macroscopic and microscopic structure of bone, the formation of bone tissue and different types of bone cells will also be introduced. In this chapter, the functions of bone cells and bone adaptation processes will be discussed. In the next chapter (Chapter 3), osteoporosis and the factors related to osteoporotic fracture, demographic features, and available methods for evaluating the osteoporotic fracture risk in research will be reviewed. The epidemiology and etiology of osteoporosis will be de-

scribed in this section. In addition, the different types of hip fractures according to their anatomical position will be briefly discussed there. The finite element method used in the previous research will also be reviewed in Chapter 3.

In Chapter 4, the construction of the finite element model, load application procedure, boundary conditions and material properties assignment will be discussed subsequently. The geometric parameter assessment for finding the correlation with the FE results will also be discussed in this chapter. At the end of this chapter, the methodology for calculating fracture risk indices (FRI) at the critical sections will be demonstrated.

In Chapter 5 and 6, the results from finite element modeling will be discussed thoroughly. In the beginning of Chapter 5, the validation of the code will be presented followed by the results for the test cases. The mesh convergence test and the region width sensitivity test will also be presented there. In this chapter, the factors affecting the accuracy of finite element results will be discussed. The influence of different parameters like body weight, bone density or length of femur etc. on FE results will also be discussed.

In Chapter 6, important outcomes and the limitations of the study will be discussed. Recommendations for improving the finite element model by minimizing the related errors will also be discussed in this chapter. The minimization of errors and the implementation of this process in monitoring the osteoporotic fracture can be considered as possible future works.

Chapter 2

Bone Structure and its Physiology

Bone is the rigid organs that constitute part of skeleton of vertebrates which provides the internal support of the body and protects the vital organs. Bones move and support various organs of the body. Bones come in a variety of shapes and have a complex internal and external structure. The femur is the most proximal bone of the leg in biped vertebrates and is established for walking or jumping. It is the longest as well as the largest bone of the human body. It has been found that, on average a male femur is 48 cm long with a 2.84 cm mid shaft diameter.

In this chapter, a brief description of bone as a biological tissue with shapes and mechanical behaviour will be presented. After describing the shapes and structure of bone especially the femur, a short description of bone adaptation process will be introduced. In the last section of this chapter, osteoporosis, the metabolic disorder of bone due to decrease of bone density and strength, will be discussed.

2.1 Bone Tissue

Bone belongs to the interstitial tissues (supportive tissues) but differs from other tissues by its high content of inorganic salts giving a comparatively high strength. It is also a dynamic tissue that continuously undergoes remodeling which is a replacement process of old bone by new bone with little change in shape. Bone, the rigid part of the body, has two types of tissue macroscopically. These two main categories are: Trabecular or Spongy bone and Cortical or Compact bone. Trabecular bone is composed of a network of trabeculae located at the inner parts of flat bones and at the ends of long bones. Its high porosity usually varies between from 0.75% to 0.95% [21]. The spaces between the bone trabeculae contain bone marrow. Trabecular bone attains its maturity during a process called modeling. It has a larger surface area and undergoes greater remodeling, and is therefore more responsive to changes in mineral metabolism than cortical bone. Cortical bone is the dense tissue which contributes about 80% of the weight of the human skeleton with a very low porosity of 0.05% to 0.10% [21]. It facilitates bone's main functions which are primarily found in the shaft of long bones. The canals and passageways riddled with the cortical bones are served as channels for nerves, blood vessels and lymphatic vessels microscopically [22]. Figure 2-1 shows the cortical and trabecular bone present in the proximal femur in the coronal section.

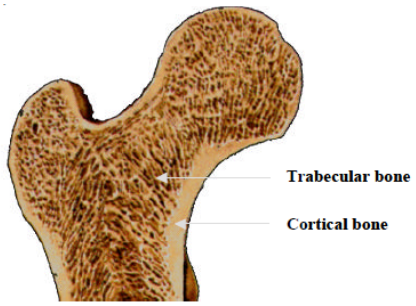

Figure 2-1: A coronal section through the proximal femur showing trabecular bone enclosed by cortical bone [23]

Bone Cells:

Bone cells are the smallest part of bone mass (i.e. only 5% of total bone mass) with distinct functional features. These include osteoclasts, osteoblasts and osteocytes; each of them plays a central role in the regulation of bone remodeling.

Osteoclasts are large bone cells formed in the marrow of the bone. These cells are made from fused cells and have multiple nuclei with a similarity in structure to white blood cells. They are responsible for breaking down bone tissue; these bone cells perform an important role in bone growth and healing. On the other hand, osteoblasts are the bone cells responsible for the creation of new bone. Working collectively, osteoblasts produce unmineralized bone matrix called osteoid from collagen and other organic moieties. Calcium and mineral deposits on the osteoid giving the bone its rigid structure. Osteocytes are responsible for proper development and maintenance of the skeleton, as well as regulating levels of minerals present in the bloodstream and throughout the body. Osteocytes constitute approximately 90% of bone cells in the adult skeleton. They act as a mechanosensors in bone, sensing physical strains and micro damage, and initiating the appropriate modeling and /or remodeling response [24]. In brief, osteoclasts resorb bone, os-

teoblasts form new bone material, and osteocytes are assumed to play an important role in calcium regulation [25]. These three types of bone cells are presented in Figure 2-2. Lining cells and osteogenic cells, though both derived from osteoblasts, also have their own key functions for proper bone health.

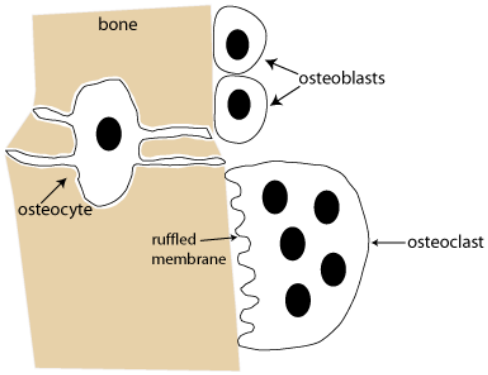

Figure 2-2: Different types of bone cells [26]

2.2 Bone Adaptation: Modeling and Remodeling

The structure of bone is designed to support loads produced by daily activities and locomotion. Bone has the ability to change its external geometry and internal architecture gradually. It is a remarkable material which undergoes a process to increase its strength and resists daily by adapting its mineral and geometry, called bone remodeling. The principle of this functional adaptation is described by "Wolff's law" (Wolff, 1892), named after the medic Julius Wolff (1836-1902). According to this law, "every change in the form or function of a bone is followed by adaptive changes in its internal architecture and external shape". The adaptive process consists of both internal and external remodeling.

Internal remodeling is a change of density and structure of bone whereas external remodeling specifies an evolution of the bone shape by redefining the external geometry [27]. But physiological external remodeling is hard to prove clinically as in most cases it is due to pathological circumstances. Generally, external modeling develops more slowly than internal modeling, especially for adults [28].

The modeling and remodeling processes are not very different at the cellular level. They are based on the separate actions of osteoclasts and osteoblasts, respectively. Bone modeling is the process of attaining mature morphology of bone during growth whereas remodeling is the continuous renewal of mature bone tissue by local bone resorption and subsequent formation. Bone remodeling or bone metabolism is a dynamic and life long process and helps to maintain bone strength and mineral homeostasis. This remodeling is necessary to allow the skeleton to increase in size during growth, respond to the physical stresses placed on it, and repair structural damage caused by fatigue or fracture. It consists of the removal of bone by the osteoclasts, followed by the synthesis and mineralization of new bone matrix by the osteoblasts within the cavity created. The remodeling cycles usually starts when injury or mechanical stress occurs in bone [29]. Under normal circumstances the sequence is always that of resorption followed by formation, and the amounts of bone resorbed and formed within individual remodeling units are closely balanced [30]. It is stated in the literature that a coupled mechanism must exist between bone formation and resorption [29].

In the case of bone modeling, the formation and resorption are not balanced, which causes changes in micro-architecture. However, the cellular activities of osteoclasts and

osteoblasts in modeling are basically similar to those in remodeling. Beyond this, the activities of osteoclasts and osteoblasts may also be entirely uncoupled in some cases.

There are several control mechanisms working simultaneously on bone remodeling like stress/strain distribution [31]. Mechanical forces also have a major influence on the bone modeling and remodeling processes in both cortical and trabecular bone. Ruimerman *et al.* [32] developed a theory which describes the coupling between the formation and resorption as an effect of mechanical stress transfer. They established a computational model for strain-related trabecular bone remodeling and adaptation. They concluded that SED (strain-energy density) is the triggering variable in predicting trabecular morphologies.

2.3 Osteoporosis and Its Pathogenesis

Osteoporosis is a skeletal disorder of decrease in bone mass and deterioration of bone tissue with a consequential increase in bone fragility and susceptibility of fracture. It has been operationally defined on the basis of bone mineral density (BMD) assessment. A person who suffers from osteoporosis has a normal bone composition, but it is thinner than in normal individuals. As osteoporosis progresses, bone is gradually lost, leading to a reduction in the number, thickness, and connectivity of trabeculae. According to the WHO criteria, osteoporosis is defined as a BMD that lies 2.5 standard deviations or more below the average value for young healthy women (a T-score of $\leq$ 2.5 SD) [33]. The structure of normal healthy bone and osteoporotic bone is presented in Figure 2-3.

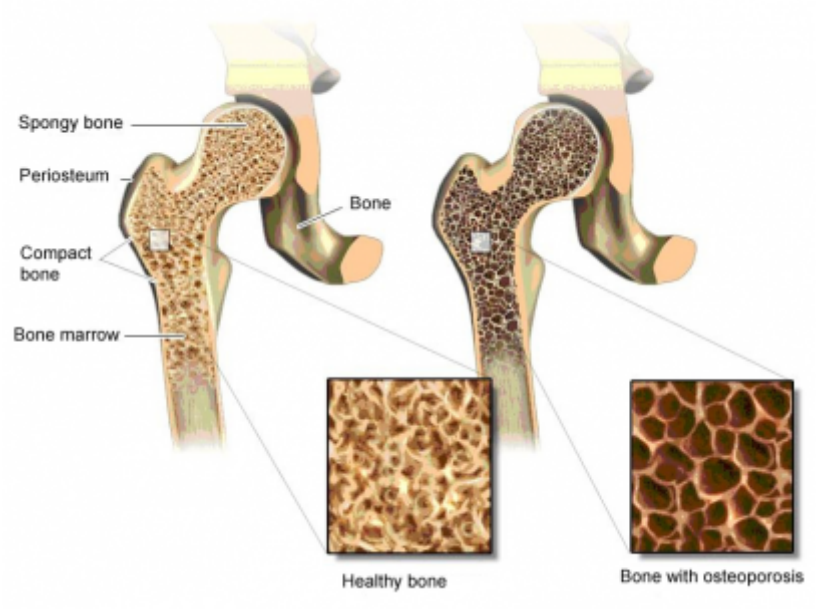

Figure 2-3: Healthy bone and osteoporotic bone [34]

The pathogenesis of osteoporosis involves a complex and multi-factorial process. Though the pathophysiology of osteoporosis is not well understood by researchers, but is obviously caused by disturbed modeling and remodeling. Disruption in bone remodeling is common in osteoporosis [35]. Skeletal development is partly responsible for the risk of osteoporosis, specifically attainment of peak bone mass and a greater amount of bone lost in later life. Normally adult bone is continuously going through bone formation and resorption processes. The mass of bone may be deficient either because resorption is too great or because formation is too little, or both. Thus, net bone loss occurs only when the rate of bone resorption (destruction) exceeds the rate of bone formation (production). Proper understanding of the morphological degeneration in osteoporosis requires knowledge of the modeling or remodeling processes. These processes are conducted by specialized bone-resorbing cells (osteoclasts) and bone-forming cells (osteoblasts). The

bone adaptation processes i.e. modeling and remodeling are discussed briefly in the previous section (Section 2.2).

Osteoporosis can be subdivided into three groups, primary osteoporosis (Type I), age related osteoporosis (Type II) and rare form of the disease (Type III). Primary or Type I or postmenopausal osteoporosis affects the women within 15 to 20 years of menopause, and approximately 5% to 20% of old women are affected [36], with a peak incidence in the 60s and early 70s. The occurrence of osteoporosis in women is up to eight times higher than that in men [37]. Type I osteoporosis is characterized by increased bone resorption due to osteoclastic activity and is generally believed to be related to estrogen deficiency.

Age-related osteoporosis, also known as senile or type II osteoporosis, occurs when there is excessive bone loss manifested after age 70 years in both women and men. Age-related bone loss begins at age 35 to 40 years when the balance shifts to favor resorption and the skeleton begins to lose bone mass [38]. In type II osteoporosis, cortical and trabecular bone is lost, primarily leading to increased risk of hip, long bone, and vertebral fractures.

Type III or secondary osteoporosis occurs equally in men and women and at any age. In men, most cases are due to disease or drug therapy. The most common causes of secondary osteoporosis include: exposure to glucocorticoid medications, hypogonadism (low levels of testosterone), alcohol abuse, smoking, gastrointestinal disease, hypercalciuria (high levels of calcium in the urine), immobilization, etc.

Chapter 3

Epidemiology of Osteoporotic Fractures

3.1 Overview

Osteoporosis and related fractures represent a major and growing public health concern for the United States and worldwide. It is estimated that about 200 million women are affected by osteoporosis worldwide, - approximately one-tenth of women aged 60, one-fifth of women aged 70, two-fifths of women aged 80 and two-thirds of women aged 90 [39]. It has been indicated in the literature that females fracture more than the males, and the occurrence of these fractures increases exponentially with age [40]. Clinically, a fracture is classified as osteoporotic if it occurs as a result of minimal trauma, such as a fall from standing height or less.

Since osteoporosis to a large extant is an age related disease [41], aging of the population has major public health implications in industrialized countries. In Canada, the prevalence of osteoporosis reported to be 21.3-27.1% in women and 5.5-6.4% in men over age

50 [3, 42]. It has been estimated that approximately 1 in 3 women and 1 in 5 men in Canada suffered an osteoporotic fracture during their lifetime [38]. A recent study shows that falls are more common in elderly people [2] and responsible for most of the hip fractures arising from osteoporosis.

The most common osteoporotic fracture sites include the proximal femur, distal forearm, and vertebrae [43]. An osteoporotic fracture often causes pain and disability. More importantly, it increases the mortality in older men and women. Vertebral fractures cause back pain, loss of height, and depression. Wrist and other fractures have considerable morbidity. Beyond this, osteoporosis and osteoporotic fracture impose social and economic burdens. The total costs of osteoporosis are difficult to assess and are based on many assumptions. There are 1.5 million fractures annually in the United States [44] attributed to osteoporosis with attendant costs exceeding $10 billion dollars per annum [45]. In the year 2008, the cost was $23.3 billion [46]. Over 30,000 hip fractures occur each year in Canada. By the year 2041, the number of hip fractures in Canada is expected to quadruple due to population aging, and the annual cost of hip fracture is expected to increase to $2.4 billion [3]. Therefore falls are regarded as an expensive problem among the older people all over the world [46].

3.2 Classification of Hip Fractures

Researchers have often evaluated risk factors for hip fractures as a homogeneous group [1, 2, 46, 47]. The risk of hip fractures is not same for all locations and varies signifi-

cantly varies among subtypes [48]. In general, hip fractures are classified by anatomic location and by fracture type. The general categories include intracapsular (femoral neck and head) and extracapsular (intertrochanteric and subtrochanteric) fractures. Hip fractures occur at three different locations of the femur, femoral neck (or cervical) fractures, intertrochanteric fractures and subtrochanteric fractures. Femoral neck fractures occur in the narrowed section of the upper femur between the rounded femur head and bony projections called trochanters, whereas intertrochanteric fractures occur in the area between the greater and lesser trochanters. Subtrochanteric fractures occur below the level of lesser trochanter.

Femoral neck fractures are common in adults over 60 years of age and occur most frequently in women. Most femoral neck fractures occur within the capsule that surrounds the hip joint and are therefore termed as intracapsular. The blood supply to the femoral head is entirely dependent upon a series of arteries that pass through the femoral neck region. Therefore, fractures of the femoral neck can entirely disrupt the blood supply to the femoral head. Femoral neck fractures are further grouped into non-displaced and displaced fractures by the alignment of the fractured segments in relation to the original anatomic position of the femur. The treatment of this type of fracture is complicated because of poor blood supply. If the displacement is minimum and blood supply is adequate hip pinning and a plate is used to fix this problem. In case of severe displacement and poor blood supply, the femoral head is surgically removed and replaced by an endoprosthesis.

Intertrochanteric fracture is a type of extracapsular fracture, and the blood supply is usually not affected by this type of fracture. These fractures occur in the area between the

greater and lesser trochanters. This is usually caused by direct trauma or force and most common in women. However, these fractures are complicated by the pull of the hip muscles on the bony muscle attachments, which can exert competing forces against fractured bone segments and pull them out of alignment. Intertrochanteric fractures may be further grouped into stable and unstable fractures, depending on the location, number, and size of the bony fragments. Subtrochanteric fractures usually are the result of direct trauma of a fall. Isolated subtrochanteric fractures occur in the area between the upper borders of the lesser trochanter to 5 cm below it. The blood supply to the bone of the subtrochanteric region is not as good as the blood supply to the bone of the intertrochanteric region and thus heals more slowly. Subtrochanteric fractures are also subject to competing forces exerted by muscular attachments on the femur that tend to pull the fractured fragments out of alignment. Locations of femoral neck fracture, intertrochanteric fracture and subtrochanteric fracture are illustrated in Figure 3-1.

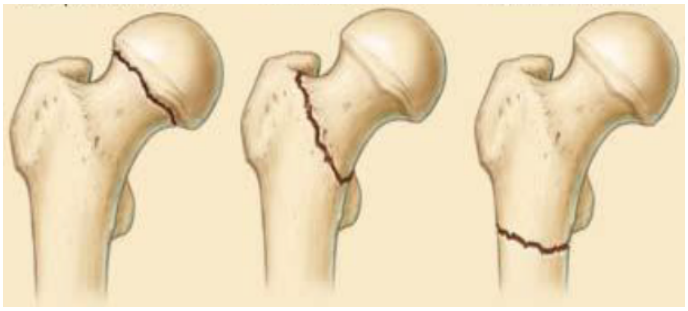

Figure 3-1: Different types of hip fracture (femoral neck fracture, intertrochanteric fracture and subtrochanteric fracture) [49]

Patterns and trends among different types of hip fractures vary. For example, the rate of femoral neck fracture of elderly women is higher in the UK and is similar for the population of Australia. Both in Japan [50] and USA [48, 51, 52], intertrochanteric fractures oc-

cur more frequently than femoral neck fracture in elderly people. In addition, the rate of subtrochanteric fracture is less than other two types of fracture. From the study of Michelson *et al*. [53], it is found that in USA, 49% of hip fractures are intertrochanteric, whereas 37% are femoral neck and 14% are subtrochanteric fracture. These data are consistent with those of Margaret *et al.* [51] and Hinton *et al.* [48, 52] with a small difference (3%) in the subtrochanteric fracture. By definition, these are the only possible fracture sites.

3.3 Demographic Feature of Hip Fracture

The main demographic risk factors for osteoporosis and osteoporotic fractures include increased age, female gender and white race. Low energy trauma is mainly responsible for most fractures in middle aged and old people [1].

There is significant racial difference in osteoporosis and in the incident of osteoporotic fracture. In USA, post menopausal osteoporosis has repeatedly been noted to be more common in non-Hispanic white women and in Asian women than it is in African-American women [5, 54]. This may be explained by the higher peak bone mass achieved before the menopause in African-American women. Asian women have lower bone mass than white women, but, interestingly, the rate of hip fractures is not proportionally higher, sometimes it is lower (40-50%) than white women [55]. Areal BMD measured from DXA is lower in the Asian women than from Black or Caucasians which is mostly related to their body size [56]. Asian women are shorter than Caucasians or African Ameri-

cans and have lower aBMD as it is influenced by bone size. The lower rate of fracture in Asian women is paradoxical and a shorter hip axis length might be a major factor accounting for Asian women's lower risk of hip fracture [57].

Stress fractures are completely different [58]. There is a sharp increase in the number of femoral neck fractures with age, and more in women than in men in UK, found by Gallannaugh *et al*. [59]. In women aged 60 to 64 years, the incidence was 1.08 per 1000 population and rose to 32.76 at 90 to 94 years of age. It was 20.00 per 1000 in men by the age of 95 years and over. Fisher *et al.* [60] studied the site specific epidemiology of hip fracture in the Australian capital territory and found of all hip fractures, 55% were cervical, 41% closed trochanteric and 4% closed subtrochanteric. The overall ratio of cervical to trochanteric fracture was 1.3 [60]. The cervical to trochanteric hip fracture ratio in Ecuador [61] is also similar to that of Australia (2.5 for women and 1.5 for men) but an opposite trend was observed in the Japanese population [62] by a survey for 10 years (femoral neck fractures less common than trochanteric fracture). Lofman *et al.* [50] studied the influence of age, gender and fracture types on hip fractures in Sweden and reported that age is higher for cervical fractures compared to trochanteric fractures amongst men. In contrast, in women, the influence of age is higher for trochanteric fractures than cervical fractures [50]. Tanner *et al.* [63] studied in Ontario, Canada and observed that over 5 years the proportion of intertrochanteric fracture increased from 41.5% to 50% for all patients, rising significantly for women with age but decreasing for men.

3.4 Methods of Evaluating Hip Fracture Risk

3.4.1 DXA Imaging, Areal BMD and T-score

The WHO (World Health Organization) describes DXA (Dual Energy X-ray Absorptiometry) as the most highly developed technique and the most thorough approach for diagnosing osteoporosis. It is therefore regarded as the "gold standard", due to a better performance than other available techniques. Currently, the measurement of areal bone mineral density (aBMD) by DXA is the most commonly used non–invasive measurement for the diagnosis of osteoporosis. It is a sensitive technique which uses density measurements of the spine or hip and can sometimes detect changes in bone density only 6 to 12 months after a previous measurement is obtained [64, 65].

DXA requires remarkably lower radiation doses. Using manufacturers' data, the effective dose for lumbar spine and whole-body DXA is reported to be 1−5 μSv [66]. This is less than the dose of a standard PA (posteroanterior) chest radiograph. Scanning times are now less than 2 min for the spine, hip or forearm, and less than 3 min for the total body [67]. It is currently the most frequently used technique for diagnosing osteoporosis and estimating fracture risk [68, 69]. BMD is a major determinant of bone strength and BMD values obtained at the proximal femur and lumbar spine are used to diagnose osteoporosis by applying the criteria established by WHO.

As in all radiologic studies, DXA relies on the differential absorption of X-rays to differentiate tissues of different radiographic density. In addition, DXA can quantify (in grams)

the bone mineral content (BMC) at various body sites. By selecting regions of interest (ROI), a bone area (BA) is selected with units of square centimeters. BMC is calculated for each pixel in the region of interest (ROI) by comparing the X-ray attenuation of that pixel to a reference standard in grams. This value is divided by the pixel's area to derive the BMD of that pixel with units of grams/cm². The areas of all the pixels in the ROI are summed to give BA and thus, BMD = BMC/BA.

A typical DXA scanner is shown in Figure 3-2:

Figure 3-2 : A typical DXA scanner (Courtesy: Capital Imaging Associates) [70]

DXA has been demonstrated to measure bone density and body fat composition and has been used to evaluate the effects of pharmaceutical therapy. DXA scanners are widely available in clinics.

T-score:

The T-score is a statistical way to standardize BMD results. It is the number of standard deviations above or below what is normally expected in a healthy young person (age 20-30 years). The T-score is defined as the difference between a measured bone density and the expected young normal value divided by the population standard deviation (SD) at the corresponding anatomical sites. T-score is a unitless value, as it is a ratio of two num-

bers with the same units. At different sites of femur, the precision limitations of T-score vary as shown in Figure 3-3:

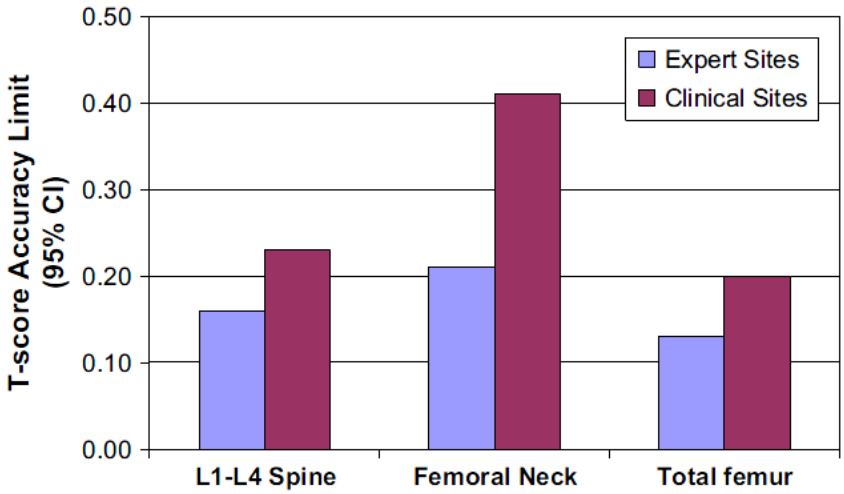

Figure 3-3: Average T-score accuracy errors (95% CIs) [71]

According to the World Health Organization, osteoporosis is defined based on the following bone density levels:

- A T-score no more than 1 SD or greater below of the young adult mean indicates normal bone density.
- A T-score of 1 to 2.5 SD below the young adult mean (-1 to - 2.5 SD) indicates low bone mass.
- A T-score of 2.5 SD or more below the young adult mean (≥ 2.5 SD) indicates the presence of osteoporosis.

The choice of this 2.5 standard deviation cut-off by the WHO was based on epidemiological data and it was based on comparable life time fracture risk.

3.4.2 Computed Tomography and Volumetric BMD

Computed Tomography (CT) is a powerful non-destructive evaluation technique for producing three-dimensional (3D) cross-sectional images of an object. It is presently the accepted method for the measurement of volumetric Bone Mineral Density (vBMD), expressed in units of mg/ cm^3. Contrary to the planar method used in DXA examinations, CT uses X-rays from multiple angles to generate and reconstruct 3D-image datasets of the scanned object, based on its X-ray absorption. Volumetric quantitative CT (vQCT) provides 3D information of bone. Materials with large atomic numbers and higher material densities have higher X-ray attenuation. The level of X-ray attenuation is expressed as CT numbers, measured in Hounsfield units (HU). After being calibrated with scan phantoms, HU is used to calculate the bone mineral density. Information of the internal structure of an object such as dimensions, shape, internal defects, and density are readily available from CT images. DXA remains the predominant screening tool for evaluating fracture risk because of its lower radiation dose and cost, but the use of quantitative CT has increased in recent years due to its ability to separate cortical and trabecular bone and ablity to provide true volumetric density [72]. Though areal bone mineral density measured from DXA has a strong correlation with hip fracture risk [73, 74], it is not able to provide detailed anatomic information of the pathophysiology of hip fracture [57]. On the other hand, quantitative CT (QCT) provides information on bone size such as tissue volume and cross sectional thickness along with the trabecular cortical volumetric BMD [75, 76]. Trabecular bone has a higher turnover rate than cortical bone due to its greater sur-

face area and this makes QCT a very useful technique to monitor bone turnover and the efficacy of the treatment. Nowadays, vQCT has become an increasingly important clinical research tool in analyzing hip fracture risk. With QCT, a finite element (FE) model can be constructed by assigning 3-dimensional density measures and mechanical properties. The models can be constructed from CT data with high accuracy. QCT is a computationally expensive method for capturing 3D data which limits its usefulness for a large number of patients by increasing the computational times. Radiation dose in QCT is also significantly higher than that in DXA. Moreover, most CT based models have focused on fracture loads rather than fracture types [19, 77]. QCT may provide a more accurate BMD measurement than DXA as it avoids the effect of degenerative disease and extraneous calcification. In addition to measuring the cortex, vQCT is a sophisticated tool to determine geometrical parameters of mechanical relevance.

3.4.3 Hip Structure Analysis (HSA)

Hip Structure Analysis (HSA) has been used for strength information in a large number of studies using conventional DXA [12]. HSA programs are now commercially available and can be used to assess the geometric and structural variables of femur automatically. The structural geometry of the proximal femur can be measured *in vivo* using the specialized Hip Structure Analysis (HSA) software. The effect of changes of BMD due to changes in mineralization cannot be distinguished with the conventional measurement of BMD. Currently, tissue composition analysis is conducted mostly by invasive means.

The HSA program measures not only the BMD of the hip bone but also the structural geometry of DXA cross-sections traversing the proximal femur at specific locations [12]. It is possible to extract the X-ray absorption data from the output image data file and then calculate the amount and distribution of bone using HSA [78, 79]. The method employs the principle that a line of pixel values across the bone axis corresponds to a cut plane traversing the bone at that location and contain some of the information about the cross-section. HSA software can also be used to derive variables from the DXA scans at the narrow neck (NN), intertrochanter (IT), and shaft (S) regions. It can employ any linearized, frontal projection, X-ray or gamma-ray image of the hip. The age trends, racial and sex differences, and effect of treatment have been investigated with HSA [12, 80, 81, 82, 83].

The main limitation of this method is the use of DXA images. DXA scanners have excellent precision when used as designed for measuring BMD, but they were not designed to measure geometry [84]. Small changes in femur rotation have a large effect on the projected dimensions from which the geometry is measured. Though HSA provides some critical insights into fragility mechanisms, it is not superior to BMD in hip fracture prediction [85]. The reproducibility of HSA not good as that for conventional DXA analysis and the results are more operator-dependant [78]. Precision in measuring structural parameters of paired images using HSA is worse than conventional BMD due to positional imprecision [86]. Difficulty in precisely locating the edge margin from blurred and noisy DXA images is another important limitation of HSA [84]. In addition, this method assumes average tissue mineralization which sometimes underestimate or overestimate of geometry.

3.4.4 FRAX®

FRAX® is the tool developed by World Health Organization (WHO) used to evaluate the 10-year probability of bone fracture based on multiple cohort studies. It has become a standard for fracture prediction and integrates clinical risk factors and bone mineral density at the femoral neck to estimate the 10-year probability of fracture in patients [87]. Based on age, gender, personal and parental history of fractures, medical history, and lifestyle factors, FRAX® produces a 10-year probability score of major osteoporotic fractures and hip fractures [88]. The FRAX® model has been developed from population-based cohorts from Europe, North America, Asia and Australia. FRAX® models were internally and externally validated [89, 90]. When a model is validated from a stratum of the same population, then it is called internal validation. The external validity concerns the extent to which the results are true for new cases, for example different populations. FRAX® does not take into account falls and fall related injuries, even though falls are critically important for hip fracture [91, 92]. Falls may one day be included in FRAX®, but data need to be collected in a systematic way and must be validated for optimal performances.

3.4.5 Finite Element Analysis (FEA)

Finite element analysis (FEA) is widely applied in validation of new designs. FEA has long been used by mechanical engineers in the design of bridges, buildings, and other

structures. For modelling mechanical loading of various engineering structures provided with prediction of displacement and induced stress distribution due to applied load, FEA is effective and widely used computer based simulation technique. In the design or modeling of a physical phenomenon, FEA has become an indispensable tool. It relies on the decomposition of the domain into a finite number of sub-domains (elements) for which the systematic approximate solution is constructed by applying variational or weighted residual methods [93]. For a complete description of the mechanical behavior of a structure, a finite element analysis requires knowledge of the geometry, the material properties, and the loads acting on the object. Model geometry is usually obtained directly from the object, whereas loading conditions are measured or estimated according to the intended use of the structure. The object is described as a connected set of simple-shaped elements that attributes the related mechanical properties. The mechanical properties are derived from mechanical tests of the materials making up the structure under appropriate loading conditions.

The finite element method was introduced to biomechanics in 1972 to evaluate stresses in human bones [94]. Since then, this method, along with newly invented digital imaging techniques, has been actively used to investigate bone strength and to screen osteoporosis. FE model also facilitates investigation of the effect of changes in bone geometry and properties with an additional dimension of studying a range of loading conditions. The finite element models used in evaluating osteoporotic fracture risk are discussed in the next section.

3.4.6 Previous Finite Element Models for Assessing Osteoporotic Fracture Risk

From the literature review, it is found that 2D and 3D models have been constructed from either DXA or CT images for estimating fracture load or femur strength. Three dimensional FEA from 2D BMD images has the potential to significantly increase the accuracy of fracture load assessment [95], though sensitivity of 2D and 3D finite element analysis are statistically equal, but significantly higher than currently available method like aBMD [96]. For the FE simulations, different commercially available software like ANSYS, ABAQUS, BONEMAT or in-house computer codes developed using MATLAB, C, etc. are usually used. The material properties over the entire bone are inhomogeneous and the distribution of this inhomogeneous material property is one of the key issues for creating a subject-specific FE model. In this section the relevant research and findings in the area of osteoporotic fracture risk at the proximal femur using finite element analysis will be discussed.

Buijs *et al.* [97] used a two dimensional finite element model derived by the projection of quantitative computed tomography (CT) scans of human cadaveric femora. The properties of the femur were calculated from the projection of images by MATLAB codes. A finite element analysis of the 2D model was then developed using the commercial software ANSYS. Femoral fracture testing was carried out in some of the cadaveric femora to validate the results. By using digital image correlation, the strain distributions were

calculated from recorded high speed video of the fracture procedure and were validated against the finite element results.

Keyak *et al.* [19] developed a model which can predict fracture in the cervical and sub-capital regions and which was validated by experimental results. The construction of their model was similar to Buijs *et al*. [97] (using CT images of cadavers) with the exception that the model was three-dimensional. Elastic modulus, density and ultimate strength were calculated from ash density using calibrated CT scan data. After that, finite element analysis was completed with ABAQUS using distortion energy failure theory.

Thevenot *et al.* [98] used a semi-automatic algorithm in MATLAB and applied it to segment trabecular and cortical bone from the radiographs of cadaver femora. They generated two different models for the analysis. One of the models had only two different Young's moduli, one for the trabecular bone and another for cortical bone. Another model had one Young's modulus for cortical bone and four different moduli for trabecular bone. Using von Mises stress distributions, cervical and trochanteric fractures were determined with a satisfactory accuracy (comparing with experimental results).

Cody *et al.* [99] used quantitative computed tomography (QCT), dual energy X-ray absorptiometry (DXA) and finite element analysis (non-invasively) to predict fractures. A group of femora was used to predict femoral strength *ex-vivo*, whereas another group was used to authenticate the models from the *in-vivo* results. Their results include a three important statistics as: cross validation correlation, shrinkage on cross section and assessment of the reliability of the models.

Viceconti *et al*. [100] proposed a method to predict risk of bone fracture based on BMD (from CT image) and 3D finite element analysis. In their study, all the processes for FE

mode including mesh generation, material model and simulation were performed using the MATLAB programming environment. A loading condition onto the greater trochanter from the standing height was employed to simulate a fall. The result showed a peak strain at the femoral neck region which agrees with the available experimental results.

Testi *et al*. [101] also developed a two dimensional finite element model from DXA image and their work is quite similar to this current research. The important outcome of their work was validation of their FE results *in-vitro*. In addition, the results were also compared with a three-dimensional finite element model and a good agreement was found. They simulated a side fall onto the greater trochanter which was similar to the current study though the procedure of loading was different. Instead of using a fixed force, in the current research patient body weight was used and the dynamic effect due to falling was also considered. Their study was also limited to prediction of fracture risk at the femoral neck. More importantly, a linear correlation between the density and mechanical properties (Young's modulus, yield stress) was chosen in their study, which is not consistent with the experimental results [102, 103]. Different fracture risk indices were also defined in this current study.

Chapter 4

Image Based Finite Element Analysis

4.1 DXA Based Finite Element Modeling

Based on the available literature, an improved DXA-based finite element modeling procedure is introduced in this chapter. The design of the model was initiated with the selection of the subjects. In-house MATLAB codes were used to construct the contour of the proximal femur by extracting necessary information from the DXA images of the corresponding subjects, generate a 2D mesh from the contour, assign material property and apply loading and constraint conditions for simulating a fall on the greater trochanter. Finally, fracture risk at the femoral neck, the intertrochanter and the subtrochanter was calculated from the finite element results. The total process is described in detail in the following sections.

4.2 Selection of Subjects

In total, 180 cases were analyzed in this study where all subjects were white females. The DXA images were collected from the St. Boniface Hospital, Winnipeg, MB using 'Lunar Prodigy'. The cases were randomly selected from the Manitoba Bone Mineral Density data base program. To assess the relationship between finite element results with the geometrical parameters and density of the bone, all cases were considered as a single group. Body weights, total hip BMD values, BMD values at femoral neck and trochanter, and neck angles were also obtained from the image files. Body weight was considered as the applied loading in the analysis. Instead of directly using the available BMD values, neck angle or length documented with the images, these were calculated during the finite element analysis assuming a non linear relationship between the DXA images and the converted JPEG format. The characteristics of subjects are given in Table 1. The subjects were all white females, ages 26 to 79 years, with a weight from 72 to 219 pounds. Only the weight and BMD values (calculated from images) were used in this study. The body weights of the patients were applied as the loading condition of the finite element analysis, whereas BMD values were used as mechanical properties to calculate the fracture risk of the patients. The ages and heights were not used in this study, though they are used for predicting fracture risk in other techniques (e.g., FRAX®).

Table 1: Characteristics of subjects (180 cases): Mean and standard deviation of age, weight, height and BMD of the test cases

Parameters	Mean Value (Standard deviation)
Age (years)	65.93 (8.65)
Weight (kg)	61.65 (13.77)
Height (cm)	159.5 (5.6)
BMD (g/cm^2)	
Femoral Neck	0.7336 (0.1343)
Intertrochanter	0.5803 (0.1512)
Total Hip	0.7436 (0.1585)

4.3 Data Extraction from DXA Images

All data required for constructing a finite element model were extracted from DXA images which were obtained in JPEG format. The process consists of the extraction of geometric data (finding the contour) and material property data. The contour extraction includes edge detection, femur head isolation from the pelvis, and obtaining the boundary coordinates. The methodology for these tasks was developed by previous research conducted in our group [104]. The codes were expanded to accommodate more functionality. For example, the previous code for extracting the edge was mainly for the image of left femur, whereas in this study the images provided by the hospital also included DXA images from the right femur. In order to use the codes, first the images of right femurs were

identified, and then a MATLAB function "fliplr" was used to flip the images vertically. The codes were then able to detect the boundary points and other parameters.

The data extraction process is briefly discussed here. The source (JPEG format of DXA image) image was imported into the MATLAB at first with a function named "imread". The true color image was converted to a grey-scale image (which carries the image intensity information) and used for calculating the density. The information from the image was stored in an array. The image was detected after performing several operations like edge dilation the boundary. As femur overlaps with the pelvis in the DXA image, it is necessary to isolate the projected femur head from the image. The isolation process is operator-dependant which prevents the process from total automation and may act as a source for error in the finite element results. Therefore, an error analysis was also performed before analyzing the test cases and is discussed in Chapter 5. After selecting the points for isolating the femur head, the user identified another four points. Two of these points were at the femoral neck region which was used to find the narrowest neck region. The procedure for identifying the narrowest neck will be described in Section 4.9. The other two points were selected at the lesser trochanter and greater trochanter which were used for detecting the intertrochanteric and subtrochanteric regions. Figure 4-1 shows the original DXA image and the proximal boundary points after edge detection and femur head isolation. The pixel value of each node after meshing was used as a density of that node. A linear correlation was assumed between pixel value and density [101, 105]. As part of the data extraction, Young's modulus and yield stress were correlated to the density using an exponential correlation.

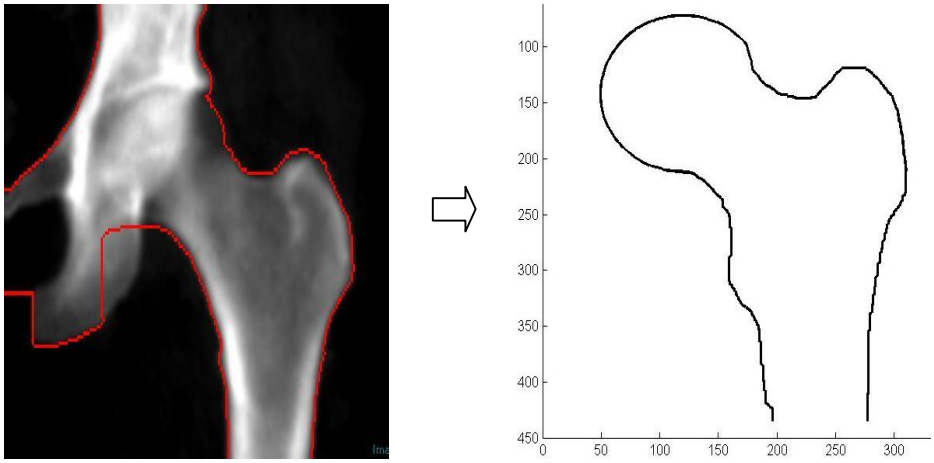

Figure 4-1: Contour extraction from DXA image

4.4 Construction of Finite Element Model

A 2D finite element model was constructed in this study as the DXA image is two dimensional. The model has a uniform thickness but inhomogeneous material properties that is projected from the 3D bone. The problem was assumed to be a plane stress problem and a three-node triangular element (Figure 4-2) was used for building the corresponding finite element model.

For a plane stress problem, the motion of material particles are described by two displacements,

$$\tilde{u}^{(e)T} = \{ \ \tilde{u}_x^{(e)} \quad \tilde{u}_y^{(e)} \}$$

The displacements are approximately expressed by shape functions ($N^{(e)}$) and element nodal displacements ($U^{(e)}$)

$$\tilde{u}^{(e)} = N^{(e)T} U^{(e)}$$

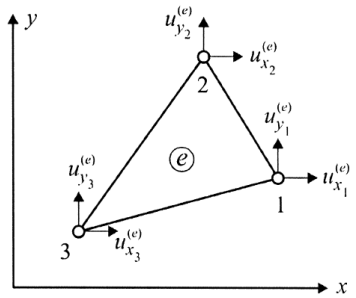

Figure 4-2: A 3-noded triangular element

For a linear triangle element, $N^{(e)}$ and $U^{(e)}$ are defined as[93],

$$N^{(e)T} = \begin{bmatrix} N_1 & 0 & N_2 & 0 & N_3 & 0 \\ 0 & N_1 & 0 & N_2 & 0 & N_3 \end{bmatrix}$$

$$U^{(e)T} = \{u_{x1}^{(e)} \quad u_{y1}^{(e)} \quad u_{x2}^{(e)} \quad u_{y2}^{(e)} \quad u_{x3}^{(e)} \quad u_{y3}^{(e)}\}$$

The shape functions expressed by physical coordinates are

$$\begin{Bmatrix} N_1 \\ N_2 \\ N_3 \end{Bmatrix} = \frac{1}{2\Delta^{(e)}} \begin{bmatrix} (x_2 y_3 - x_3 y_2) & y_{23} & x_{32} \\ (x_3 y_1 - x_1 y_3) & y_{31} & x_{13} \\ (x_1 y_2 - x_2 y_1) & y_{12} & x_{21} \end{bmatrix} \begin{Bmatrix} 1 \\ x \\ y \end{Bmatrix}$$

Where, $x_{mn} = x_m - x_n, y_{mn} = y_m - y_n$

The general expression of B-matrix for a 3-node triangle element is

$$B^{(e)} = \begin{bmatrix} \frac{\delta N_1}{\delta x} & 0 & \frac{\delta N_2}{\delta x} & 0 & \frac{\delta N_3}{\delta x} & 0 \\ 0 & \frac{\delta N_1}{\delta y} & 0 & \frac{\delta N_2}{\delta y} & 0 & \frac{\delta N_3}{\delta y} \\ \frac{\delta N_1}{\delta y} & \frac{\delta N_1}{\delta x} & \frac{\delta N_2}{\delta y} & \frac{\delta N_2}{\delta x} & \frac{\delta N_3}{\delta y} & \frac{\delta N_3}{\delta x} \end{bmatrix}$$

The previous equations load to the following specific expression,

$$B^{(e)T} = \frac{1}{2\Delta^{(e)}} \begin{bmatrix} y_{23}^{(e)} & 0 & y_{31}^{(e)} & 0 & y_{12}^{(e)} & 0 \\ 0 & x_{32}^{(e)} & 0 & x_{13}^{(e)} & 0 & x_{21}^{(e)} \\ x_{32}^{(e)} & y_{23}^{(e)} & x_{13}^{(e)} & y_{31}^{(e)} & x_{21}^{(e)} & y_{12}^{(e)} \end{bmatrix}$$

The element stiffness matrix can be obtained by using the following equation,

$$k^{(e)} = \int_{V^{(e)}} B^{(e)T} D B^{(e)} dV$$

As all entries in the *B*-matrix are constants, the stifness matrix can be written as,

$$k^{(e)} = B^{(e)T} D B^{(e)} V^{(e)}$$

In this stiffness matrix, *D* is the material property matrix. The procedure for finding *D* is described in Section 4.5.

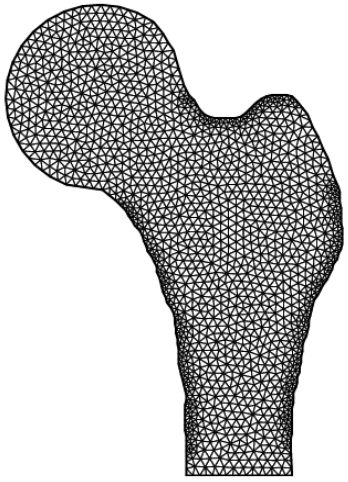

Figure 4-3: Finite element mesh of a proximal femur

Depending on femur size, the total number of nodes and elements were varied among the finite element models to achieve the same mesh density. For a larger femur, the number of nodes was about 5000; whereas the number was around 1500 for a smaller femur.

After calculating the stiffness matrix of an element, the element level force-displacement relation is expressed as follows:

$$k^{(e)}U^{(e)} = f^{(e)}$$

Once the element level force-displacement relation was formed, then the equations were assembled to form the global system of equations. The global system equations can be represented in matrix form as:

$$KU = F\,,$$

$$\text{where } K = \sum_{elem=1}^{n} k^{(e)} \text{ and } F = \sum_{elem=1}^{n} f^{(e)}$$

Here, n is the total number of elements present in the finite element model. After forming the global system equations of the finite element model, subsequent boundary conditions and loading were applied to the model. Then the global system equations were solved and important parameters such as von Mises stresses or strains were calculated.

4.5 Assigning Material Property

As bone has inhomogeneous material property, an isotropic inhomogeneous plane stress material was considered.

The material matrix, *D,* for plane stress problems is

$$D = \frac{E}{1-\nu^2}\begin{bmatrix} 1 & \nu & 0 \\ \nu & 1 & 0 \\ 0 & 0 & \dfrac{(1-\nu)}{2} \end{bmatrix}$$

Where, E is Young's modulus and υ is Poisson's ratio. Poisson's ratio was kept constant (0.3) throughout the study [101, 106]. The values of Young's modulus were extracted from DXA images and then incorporated into the finite element model.

Bone elasticity modulus was calculated from the areal bone density (ρ, in g/cm²) in the DXA image. The following empirical equation was used for calculating E (MPa) which is constructed from experimental data [102]:

$$E = 2838 \times \rho^{1.05} \, MPa$$

The bone density calculated from the image is a function of the pixel values in that image where a linear relationship was assumed between pixel value and bone density. After generating the finite element mesh, the nodal coordinates were used to find the pixel value at each node from DXA image. The density and Young's modulus at the corresponding nodes were assigned simultaneously and thus the stiffness matrix was constructed. A sample distribution of Young's modulus is shown in the Figure 4-4.

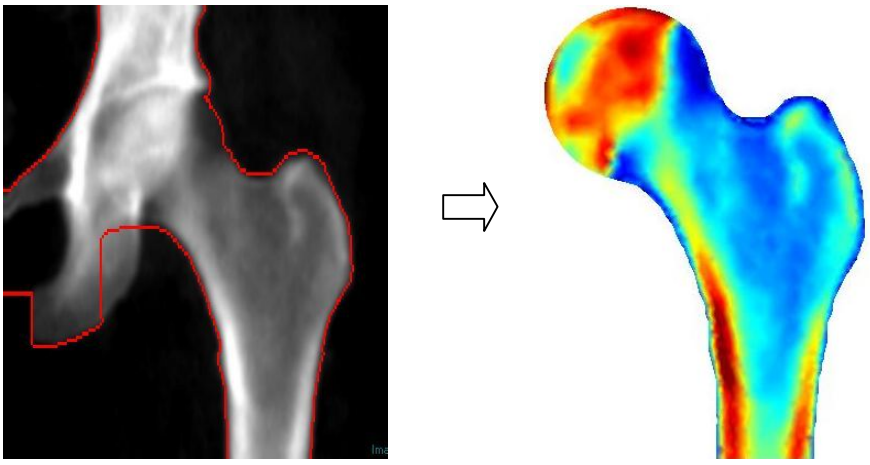

(a) DXA image (b) Distribution of Young's modulus

Figure 4-4: Assigning material property from DXA image to finite element model

4.6 Apply Load and Boundary Conditions

It is known from the literature that falling is responsible for the majority of the hip fractures in osteoporotic patients. Moreover, fall from less than standing height with a lateral orientation contributes to most fractures [107]. The loading configuration was designed to simulate a lateral fall in the patients. It was assumed that the weight of the patients is evenly distributed on the femur head as a pressure load. The femur head is the attached part of the femur with pelvis and it was selected during the edge detection. In a lateral fall, the greater trochanter contacts the ground with an impact. To simulate the dynamic effect of the fall, three times body weight of that person was considered as the loading condition on the greater trochanter [104]. It was also treated as a distributed pressure load on the greater trochanter like the loading on the femur head. For applying the load, body weight of the patient was required during the edge detection. As the provided body weights with the image files were in pounds (lb), a unit conversation had been performed before applying the load which converted weight from lb to kg. This body weight was stored in a different file in the same folder where the boundary points, femoral neck points and intertrochanteric points were stored. The boundary conditions applied to represent a fall onto the greater trochanter, were based on previously reported research [108, 98] and they are commonly accepted during mechanical tests. All distal nodes of the finite element model were made fixed both in x and y- directions. The applied boundary conditions and loading conditions are shown in the Figure 4-5.

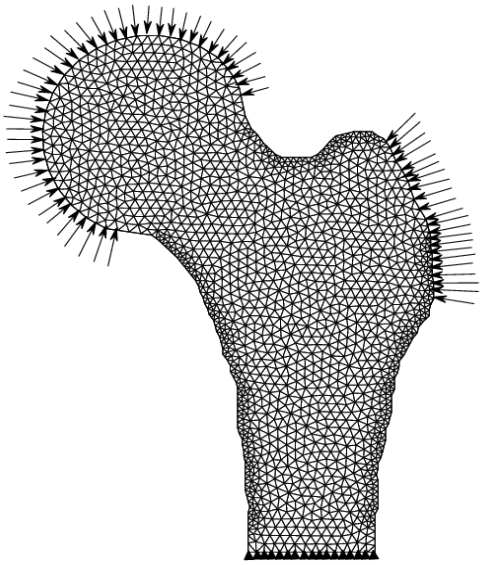

Figure 4-5: Distribution of load and boundary conditions applied on a femur

4.7 Ascertain Femoral Neck, Intertrochanter and Subtrochanter Regions for Calculating FRI

Like the femur head isolation from the hip, detecting the femoral neck and intertrochanter regions requires user participation. The user needs to detect two points at the neck region and two points at the intertrochanter during the edge detection procedure. The first step of selecting the neck region was to find the narrowest neck diameter. The two points at the neck selected by the user were used as base points for this purpose. The extreme points of the narrowest neck diameter were then identified and used further to find the femoral neck region. Selection of the intertrochanteric region was entirely user dependent. For the intertrochanteric section, user had to select one point at the middle of the lesser trochanter

and another at the top of the greater trochanter. The line joining these points was used for determining the intertrochanteric region. The subtrochanteric line was selected 1.0 to 1.5 cm distal from the point at lesser trochanter parallel to the horizontal axis. These three characteristic lines at the narrowest neck diameter, the intertrochanter and the subtrochanter are shown in Figure 4-6.

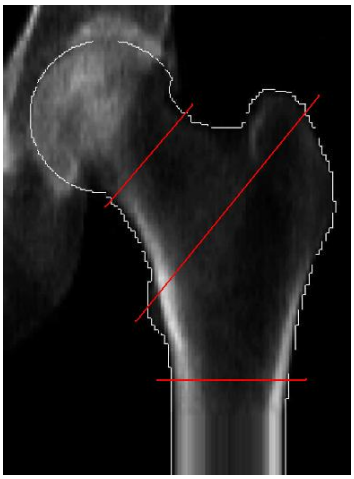

Figure 4-6: The characteristic lines at three critical sections to detect the critical regions for calculating FE results

These three lines at the critical sections are used later to select the regions at the femoral neck, intertrochanter and subtrochanter and to identify the elements inside those regions for calculating the fracture risk. The region width was finalized after performing a region sensitivity test which will be discussed in Chapter 5.

4.8 Fracture Risk Index (FRI) at Three Sections

Point-wise fracture risk index (FRI) was defined as the ratio of von Mises stress and yield stress at a node or at Gaussian point. For evaluating the nodal stresses or nodal strains, the displacement of the nodes needs to be determined. The displacement at the nodes was derived by solving the finite element equations. Since the problem was considered as a plane stress problem, all strains related to the *z*-axis were considered as zero and all the rest strains were considered independent of *z*-coordinate. For a 3-node triangular element the expression for strain-displacement relation is given below:

$$\{\varepsilon^i\} = [B]\{U^{(e)}\}$$

Where, $\{\varepsilon^i\} = \begin{Bmatrix} \varepsilon_x \\ \varepsilon_y \\ \gamma_{xy} \end{Bmatrix}$ and the expressions for $[B]$ and $\{U^{(e)}\}$ were already described in the earlier section (Section 4.4).

The expression for calculating nodal stresses is given below as a stress-stress relation:

$$\{\sigma\} = [D]\{\varepsilon^i\} = [D][B]\{U^{(e)}\}$$

$$\text{Where, } \{\sigma\} = \begin{Bmatrix} \sigma_x \\ \sigma_y \\ \tau_{xy} \end{Bmatrix}$$

And $[D]$ is the matrix for material property, which was also described in the earlier section (Section 4.5). From the nodal stresses at the *x*-axis, *y*-axis and *xy*-plane, the von Mises stress was calculated. The von Mises criterion is a formula for calculating whether

the stress combination at a given point will cause failure. Von Mises found that, even though none of the principal stresses exceeds the yield stress of the material, it is possible for yielding to result from the combination of stresses. The von Mises criterion is a formula for combining these three stresses into an equivalent stress, which is then compared to the yield stress of the material. The formula for finding von Mises stress is [109, 110]:

$$\sigma_{von} = \frac{1}{\sqrt{2}} \times \{\sqrt{(\sigma_x - \sigma_y)^2 + \sigma_x^2 + \sigma_y^2 + 6 \times \tau_{xy}^2}\}$$

The distribution of von Mises stress obtained by finite element analysis for a sample case is given below in Figure 4-7:

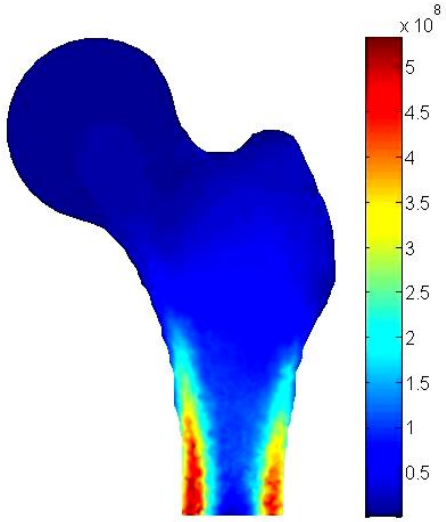

Figure 4-7: Von Mises stress distribution for a sample case

A specific region was generally considered as part of the initial step for finding the FRI at three different sections. FRI varied considerably with the width of the region, so a region sensitivity testing (convergence test of region width) was performed for solving that issue. The results from this test are presented and discussed in Chapter 5. Initially the element inside the defined region was detected by using the MATLAB function "inpoly-

gon". If the center of the element was inside the region then the element was considered to be eligible for calculating FRI. For an element inside the region, von Mises stresses and yield stresses at the Gaussian points were computed. The ratio FRI_e is then defined as follows:

$$FRI_e = \frac{\text{Von Mises stress}}{\text{Yield stress at that point}}$$

Yield stresses (σ_Y, in MPa) are also correlated to bone density (ρ, in g/cm²), by modified empirical functions that are constructed from experimental data [102].

$$\sigma_Y = 37.4 \times \rho^{1.39}$$

After calculating FRI of an element, total FRI for a section was calculated by using the following equations:

$$FRI = \frac{Q}{A}$$

Where,

$$Q = \sum_{elem=1}^{n} \int_{A_e} FRI_e \, dA$$

$$A = \sum_{elem=1}^{n} A_e$$

Here, n is the total number of the elements in the regions. Figure 4-8 shows the selected regions at the femoral neck, intertrochanter and subtrochanter which were used for calculating fracture risk index.

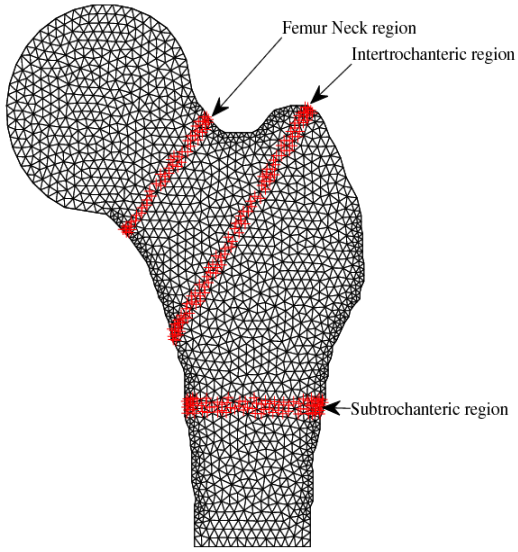

Figure 4-8: Regions selected at the femur for calculating FRI

4.9 Assessing the Geometric Parameters

The total length of the femur was measured as the distance from the top most point of the femur to the bottom most point from the finite element mesh. Since length was measured from DXA image, it was not the actual length of the femur and depends on imaging technique. The actual length of the femur is required for evaluating the effect of error in the length measurement and dynamic modeling of femur strength and will need to be considered in future work.

The neck length (NL) of the femur was measured as the distance from the right most point to the left most point on the femur. Some researchers define this as hip axis length (HAL), which is measured as the distance along the femoral neck axis, extending from the bone edge at the base of the trochanter to the bone edge at the inner pelvic brim.

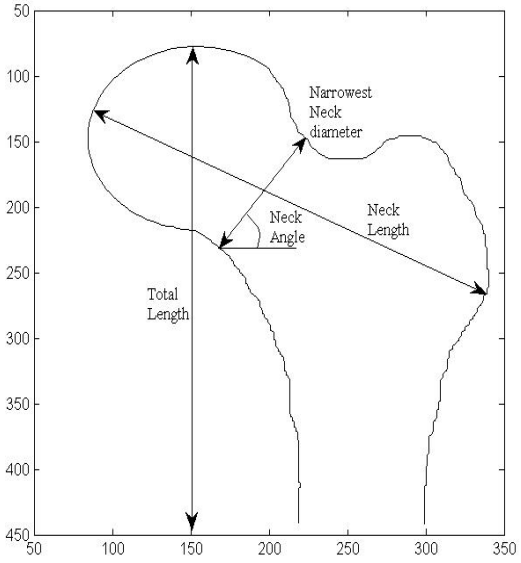

Figure 4-9: Geometric parameters measured from image

For measuring the narrowest neck diameter, a region was selected at the neck and the corresponding data points were classified into two groups based on the two sides of that region. The shortest distance between two groups was measured and defined as narrowest neck diameter. The coordinates at the end points of the narrowest neck diameter defined the slope which was considered as the neck angle.

All geometric parameters were measured before the finite element mesh, and the values were in units of pixels. It is necessary to convert length from pixels to mm to make the unit consistent throughout the study. The following relationship was used for this conversion:

$$1 \text{ pixel} = 0.2645833 \text{ mm}$$

Chapter 5

Numerical Results and Discussion

5.1 Code Verification

Verification of the code has been performed as the finite element codes were developed in-house using MATLAB. A simple cantilever beam (10mm×2mm) with a point load at the top right corner (9.375 kN) and with homogeneous material property (E = 1000 MPa, υ = 0.25) was used for this verification purpose (Figure 5-1). The reason behind this verification is that if the code is able to produce finite element results similar to those calculated from other finite element software, then it can be said that the implementation of finite element method is able to produce correct finite element results. The results obtained by using MATLAB codes were compared with the results from ANSYS (commercial finite element software). For this comparison, stresses at the mid section of the beam were computed. A convergence test for the cantilever beam was also performed as part of the verification.

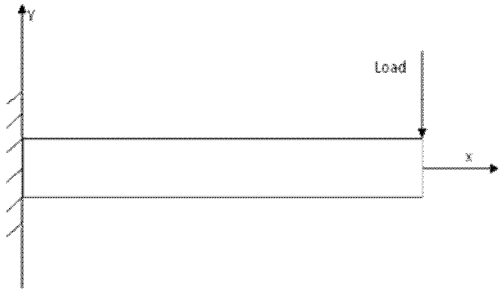

Figure 5-1: A cantilever beam with concentrated load at the top right point

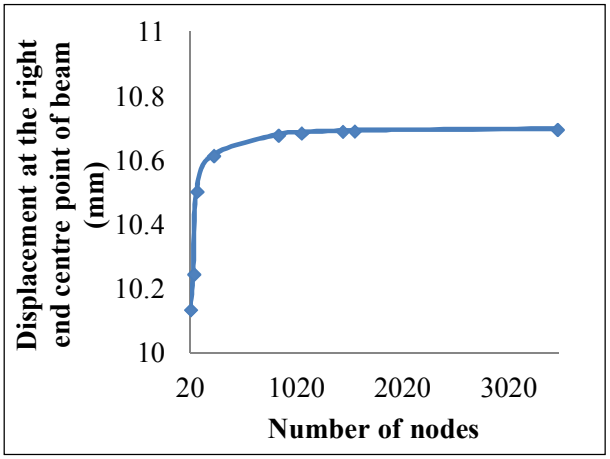

Figure 5-2: Results of convergence test (displacement at the right end centre point of the beam versus number of nodes)

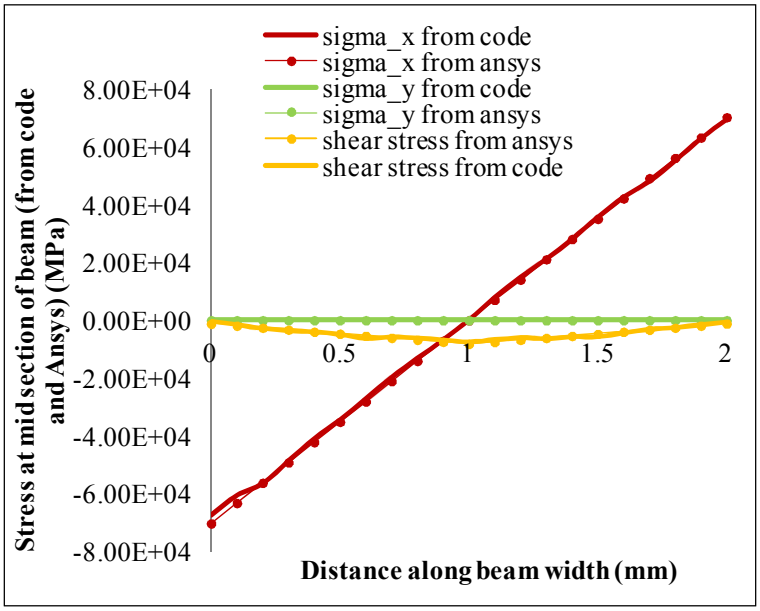

Figure 5-3: Code verification (stress distribution at the mid plane of beam from MATLAB code and from ANSYS)

Figure 5-2 shows the results of the convergence test of the cantilever beam using the MATLAB code. As the number of nodes increases, the displacement at the right end centre point of the beam converged to a steady value. The mid section of the beam (perpendicular to the horizontal axis) was chosen to compare the finite element results (stresses) derived from MATLAB and from ANSYS. The distributions of stresses (σ_x, σ_y, and τ_{xy}) from the MATLAB code were plotted in Figure 5-3. In the same figure, the distributions of the stresses computed from ANSYS were also plotted. It was found that the stress distribution from the MATLAB code and from ANSYS showed a negligible difference in σ_x (due to the difference in the mesh size in these two techniques).

After completing the validation of the code for a simple cantilever beam, the mesh convergence test for the femur model was performed, as the stress distribution is highly dependent on the characteristics of the mesh used in the analysis [111]. It was tested for one

sample case that included all three critical sections where FRI was calculated. Figure 5-4 plots the fracture risk index versus the number of nodes in the model. Slight oscillation in the convergence was present because of inhomogeneity in the material property. Eventually, the results converged at all sections with the increase of nodes (degrees of freedom).

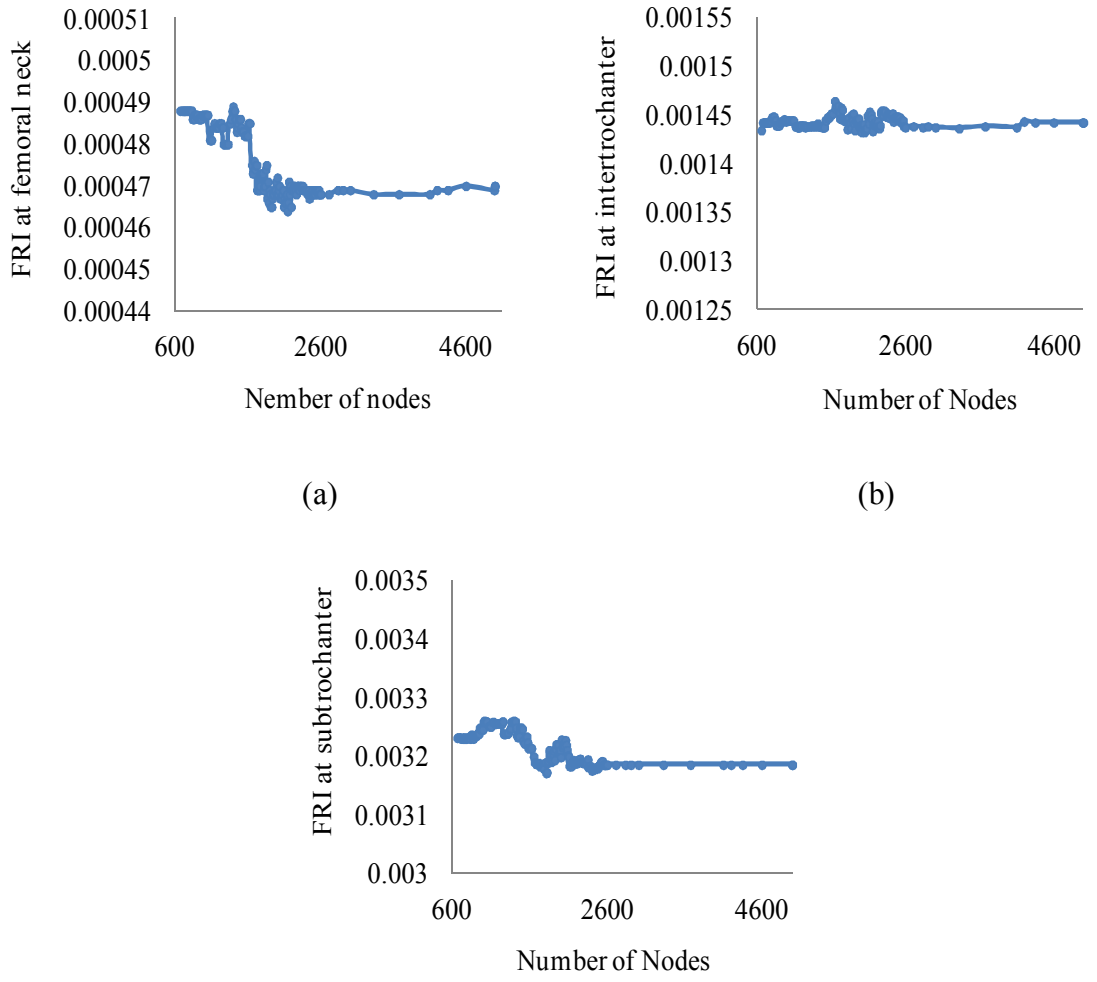

Figure 5-4: Convergence test at three sections (a) femoral neck, (b) intertrochanter and (c) subtrochanter of the femur

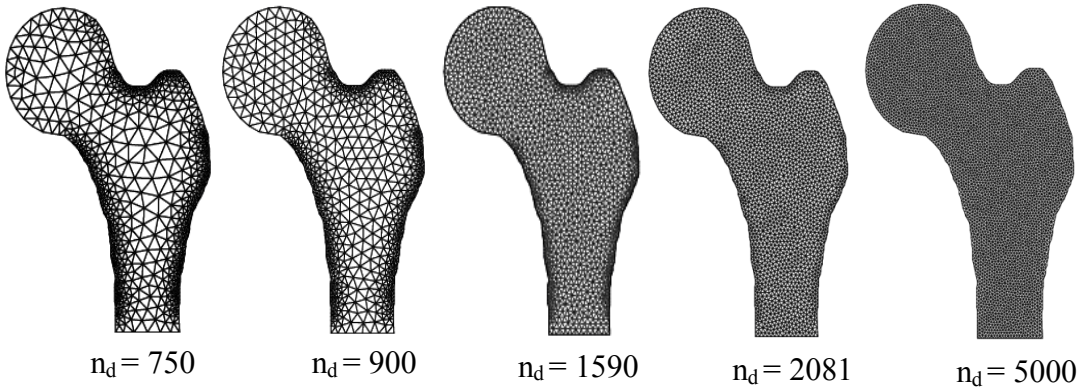

Figure 5-5: Mesh size (coarse mesh to fine mesh, here n_d is the total number of nodes)

After the mesh size convergence test, a sensitivity test of region thickness was conducted. According to the definition of fracture risk index, the thickness of the region is an important issue. For the optimum mesh size (~5000 nodes), a region sensitivity test for some sample cases at the femoral neck region was performed. For all cases, FRI calculated from the image seems to be closely related to the fracture risk index for small region. Result for one sample case is presented here (Figure 5-6). It has been also observed that the value of fracture risk index declined slightly with a decrease in region thickness. The FRI varied due to the change of the area, as it is the ratio of the average value of FRI and yield stress.

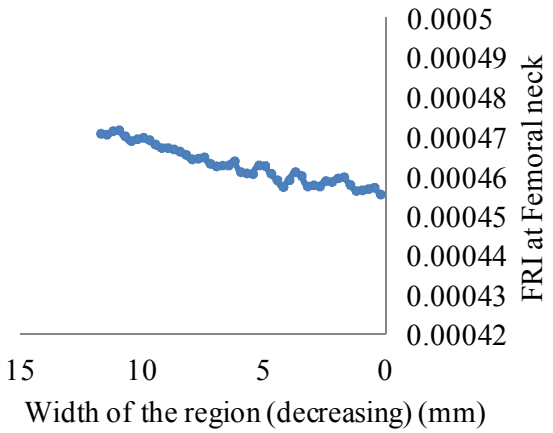

Figure 5-6: Convergence test of fracture risk index with the region thickness (at femoral neck)

5.2 Precision Study

5.2.1 Short-term Precision

Precision error is used to characterize the reproducibility of a technique. Short term precision is defined as the standard deviation (SD) of repeated measurement in a subject [112]. In this study, the FRI for two sample cases were repeatedly measured at the three specific sections- i.e. the femoral neck, the intertrochanter and the subtrochanter. The study was performed for two sample cases by selecting 3 specific points to separate the femur head followed by calculation of the FE results (referred as test 1). Then the points were re-selected and FE results were re-calculated (referred as test 2). After meshing and applying loading and boundary conditions, the model was analysed and then FRI was calculated at the three critical sections. The procedure was performed ten times and then an er-

ror analysis for the derived results was conducted. The percentage error between two consecutive results (error between test 1 and test 2, or between test 2 and test 3 etc.) was calculated. The percentages of error for all three sections varied from 0.01% to 6%. For the femoral neck section the range was 0.21% to 5.7%. The range was from 0.15% to 5.6% for intertrochanter and 0.03% to 4.6% for subtrochanter section. The variation in the finite element results (FRI) for two consecutive studies is presented in the following table:

Table 2: Effect of femur head isolation (selection of three points on femur head) on FRI

	Percentage error between two consecutive test					
	Sample case 1			Sample case 2		
	Neck	Intertro-chanter	Subtro-chanter	Neck	Intertro-chanter	Subtro-chanter
test 1~test 2	1.8099	4.02166	2.22659	2.394527	0.33746	0.30487
test 2~test 3	4.9462	0.691244	0.03275	4.571429	1.88784	2.88109
test 3~test 4	3.6876	0.61586	1.051248	1.180638	1.64586	0.02737
test 4~test 5	1.4957	0.306984	0.06566	5.49582	0.27917	0.82147
test 5~test 6	1.5184	3.766617	4.603821	0.679502	0.278396	0.32591
test 6~test 7	2.1505	0.15106	1.586274	5.70125	0.89336	0.51435
test 7~test 8	0.2145	1.99852	1.749364	3.8835	4.37189	1.48128
test 8~test 9	0.6396	1.888163	0.158781	3.322949	4.082715	1.64543
test 9~test 10	1.9565	5.6792	3.2459	4.940924	1.271421	0.1619

The mean FRI (mean absolute difference) and SD at these three sections for both cases were calculated using the repeated results of FRI. Here, the results of +/- 2 SD (for sample case 1, SD = 0.001092 and for sample case 2, SD = 0.001187) are plotted only (Figure 5-7).

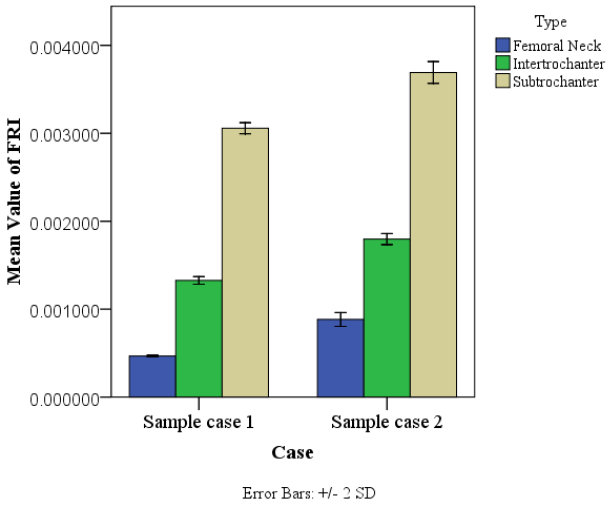

Figure 5-7: Short-term precision error of individual for two sample cases with +/-2SD

In this Figure 5-7, mean value of FRI was plotted for both cases at all three sections. It has been found that the trends for FRI at all the sections are similar. For both cases, inter-trochanteric mean FRI is higher than femoral neck mean FRI. Subtrochanteric fracture shows the highest value of mean FRI which may occur due to the selection of subtrochanteric region. The subtrochanteric region was very close to the distal end where the boundary conditions were applied.

5.2.2 Short-term Precision of Technique

Measurements of precision from a single subject may not be representative of the overall performance of the technique. A larger representative group of subjects needs to be included in the precision study. In this study a group of 28 cases was analyzed. Two DXA images for each case were analyzed using FEM. These paired images from the same person were taken within a very short time. The finite element analysis was performed for all

scans and the derived fracture risk indices for the paired images were compared. As the paired images were from the same person, their fracture load was identical as body weight was considered as the load and material and geometric property should be the same. Differences were found between the two paired images and as a consequence, variation in the finite element results appeared. To minimize error, the lengths of the paired images were forced to be the same by subtracting boundary points from the distal ends of the larger one and then the model was constructed. The relative change in FRI and relative change of density are plotted in a scatter plot (Figure 5-8). A strong negative correlation (r = -0.7528, p<0.005) between these two values was found. The relative change between the initial and follow up conditions was calculated by using the following relation:

Relative change = (Initial value – Follow up value)/Initial value ×100%

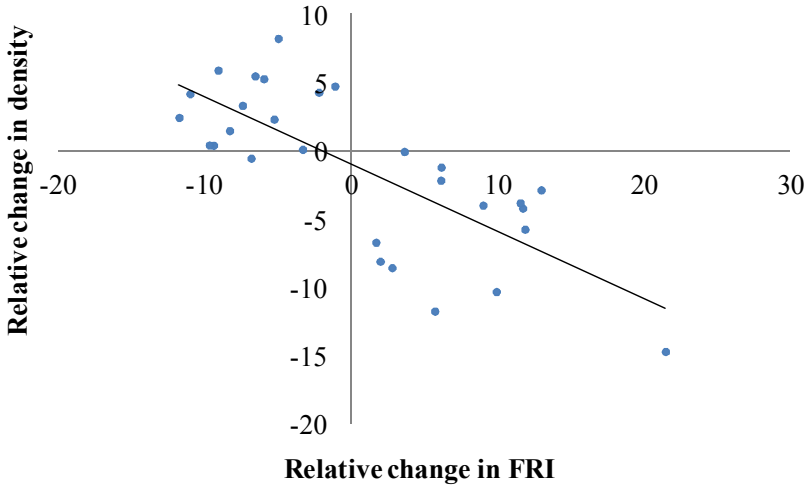

Figure 5-8: Relative change of density versus relative change of FRI for the total femur

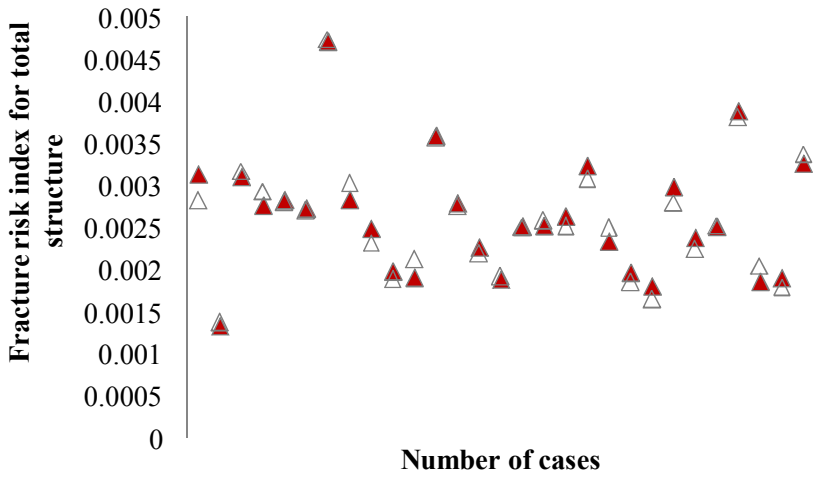

Figure 5-9: Total FRI for initial and follow up cases for precision study (△ : FRI for initial cases; ▲ : for follow up cases)

From Figure 5-8, it can be said that if the geometric parameters, applied load and boundary conditions remain same, the fracture risk index is very dependent on density (or BMD) of the femur. The fracture risk index increases with a decrease in density and vice versa. In the precision study, among the geometric parameters only the total length of the initial and follow up images were constrained to be same, while other parameters like neck length or neck diameter could be different.

Since the paired images were taken from the same person with a short time interval, FRI should be equal for each pair. From Figure 5-9, it is seen that there are apparent differences between initial and follow up FRI. This can happen due to the difference in the DXA images. Although the total length of each paired image was made equal, large differences in density between the paired images were found (maximum difference between pairs 14.65%, and absolute mean difference between density measurement 4.59%). The values of BMD (obtained with the image files from hospital) are also different for the ini-

tial images and follow up images which support the findings of density difference. A small difference in neck length (maximum difference 3.5%) and neck diameter (maximum difference between initial and follow up images 4.09%) was also observed in the paired images.

5.3 Parametric Study of Clinical Cohorts

After the completion of mesh convergence and region sensitivity tests, all cases were analyzed using the finite element code. The fracture risk index was computed for total 180 cases at the three sections. In this current study, grey-scale value at each pixel was assumed to be equivalent to BMD value at that point. The correlation between the FRI and other factors such as density and body weight were investigated.

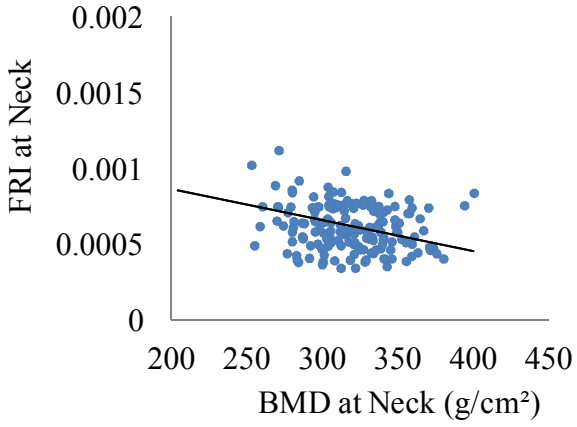

(a)

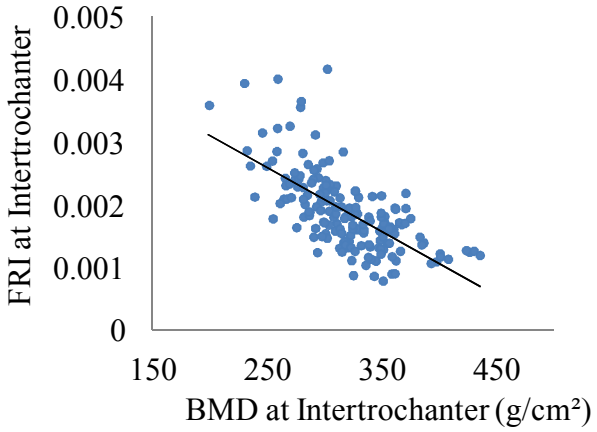

(b)

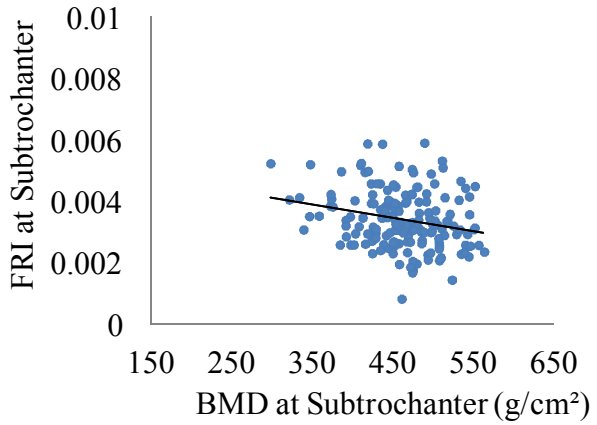

(c)

Figure 5-10: Finite element-computed FRI for fall on greater trochanter versus BMD calculated from images at three critical sections (a) femoral neck (b) intertrochanter and (c) subtrochanter

The FRI versus BMD at the three critical sections are plotted in a scatter plot in Figure 5-10.

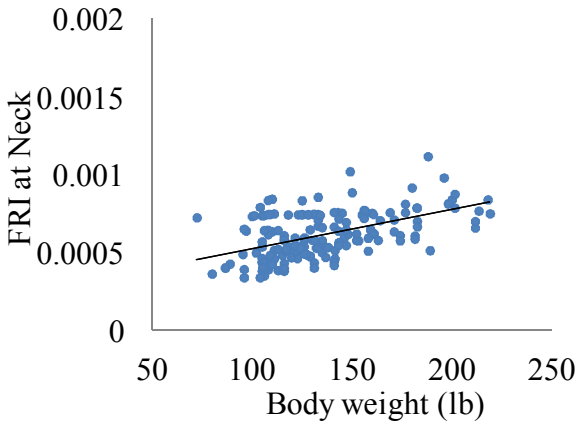
0.002
0.0015
0.001
0.0005
0
FRI at Neck
50
100
150
200
250
Body weight (lb)

(a)

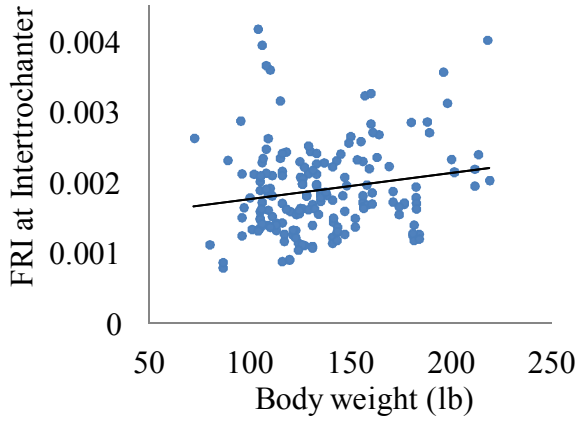
0.004
0.003
0.002
0.001
0
FRI at Intertrochanter
50
100
150
200
250
Body weight (lb)

(b)

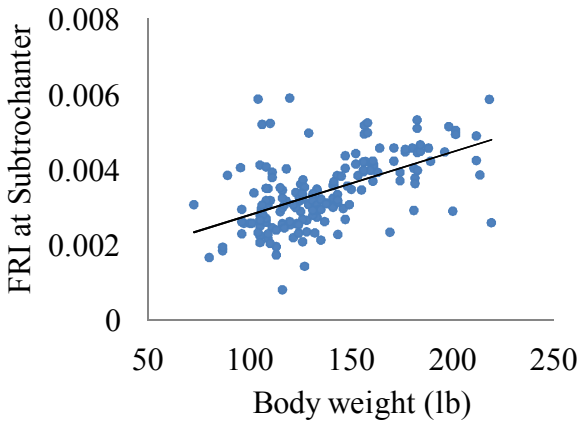

(c)

Figure 5-11: Finite element-computed FRI for fall on greater trochanter versus body weight of the patients at three critical sections (a) femoral neck (b) intertrochanter and (c) subtrochanter

The scatter plots of FRI versus body weight all three sections are shown in Figure 5-11. The effects of various geometric parameters were also investigated to show how they impact on the finite element results. The parameters used for this investigation were total length of the femur, neck length, neck diameter and neck angle. The scatter plots for fracture risk index (FRI) with these parameters at femoral neck, intertrochanter and subtrochanter sections are given in the following figures (Figure 5-12 to Figure 5-16).

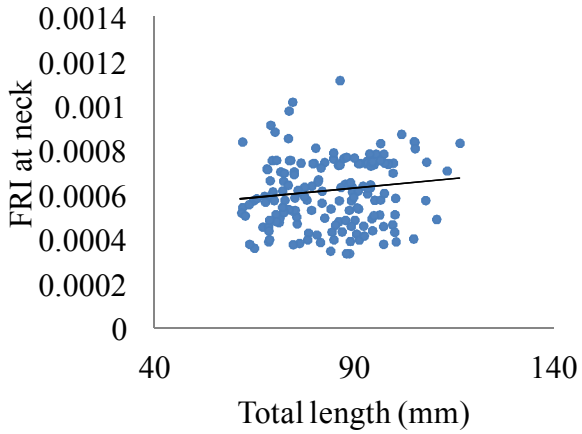

(a)

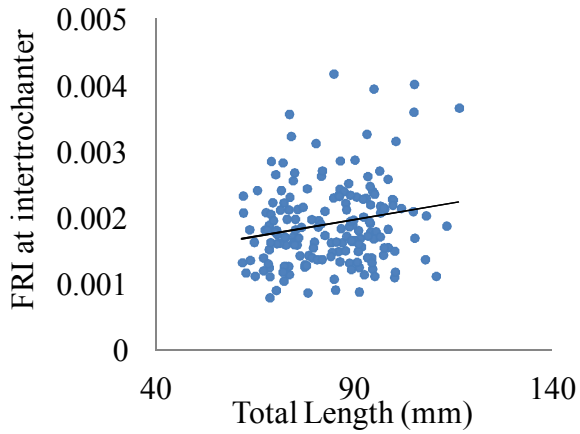

(b)

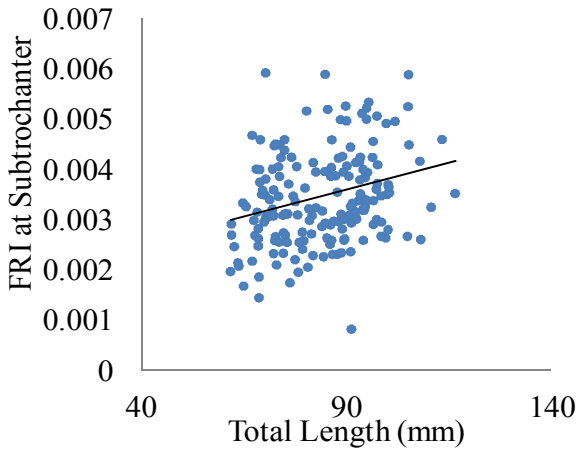

(c)

Figure 5-12: Finite element-computed FRI for fall on greater trochanter versus total length of the femur (calculated from images) at three critical sections (a) femoral neck (b) intertrochanter and (c) subtrochanter

From Figure 5-12, it is seen that FRI increases in the increase of total length of the femur at all three sections. This can be interpreted as that taller people being at higher risk of fracture as they have larger femoral length.

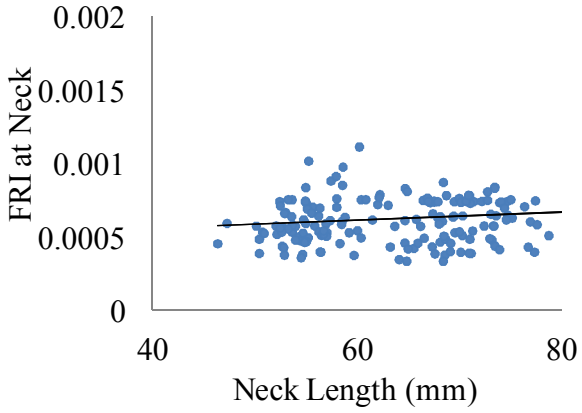
0.002
0.0015
0.001
0.0005
0
FRI at Neck
40
60
80
Neck Length (mm)

(a)

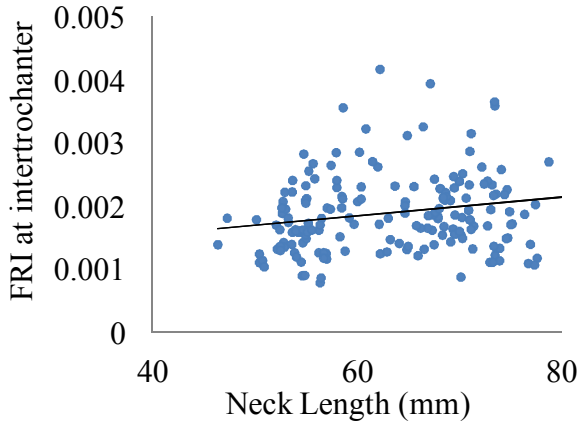
0.005
0.004
0.003
0.002
0.001
0
FRI at intertrochanter
40
60
80
Neck Length (mm)

(b)

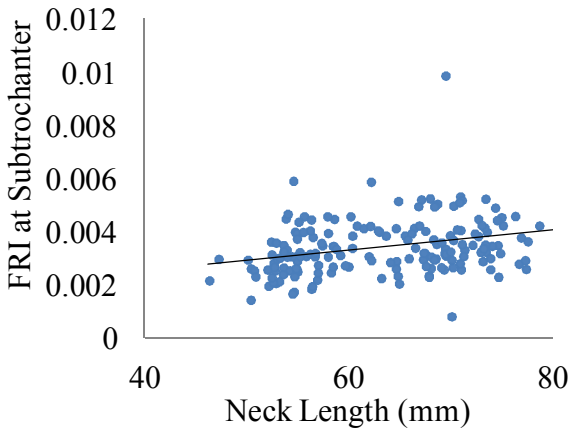

(c)

Figure 5-13: Finite element-computed FRI for fall on greater trochanter versus neck length of the femur (calculated from images) at three critical sections (a) femoral neck (b) intertrochanter and (c) subtrochanter

From Figure 5-13, it is seen that fracture risk also has a positive correlation with neck length at all sections. A larger neck length will produce higher moment at the sections when people fall and will increase fracture risk.

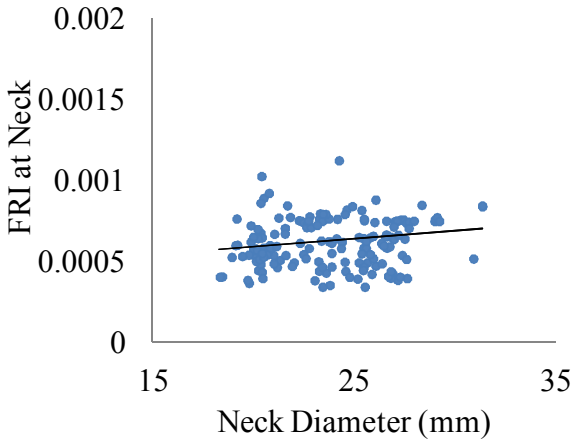

(a)

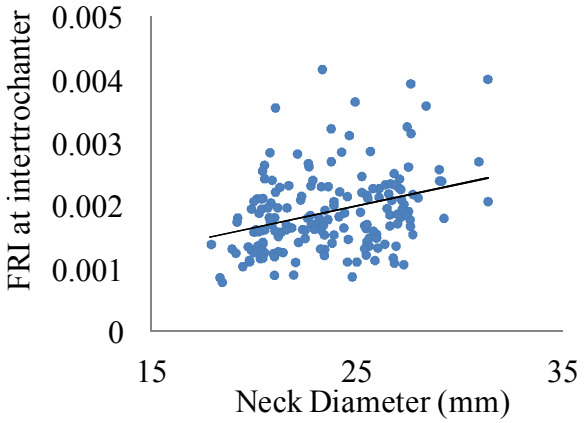

(b)

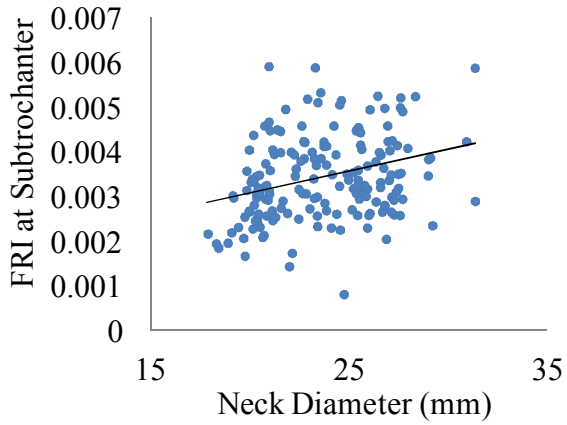

(c)

Figure 5-14: Finite element-computed FRI for fall on greater trochanter versus neck diameter of the femur (calculated from images) at three critical sections (a) femoral neck (b) intertrochanter and (c) subtrochanter

Like the total length and neck length, neck diameter shows a positive correlation with FRI (Figure 5-14). From the mechanical point of view, larger diameter of any structure should increase strength and fracture risk should decrease. But the neck diameter is not an independent variable and strongly depends on neck length. The following figure (Figure 5-15) shows the relationship between the neck length and neck diameter.

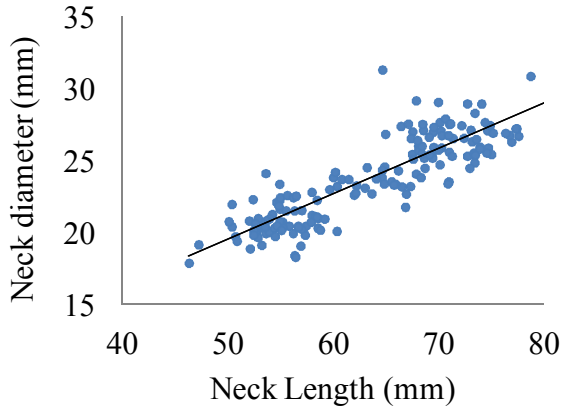

Figure 5-15: Relationship between neck diameter and neck length

As is seen from the figure, neck diameter is strongly related to neck length (correlation coefficient, $r = 0.8714$, $p<0.005$), and this likely determines the effect of neck diameter on fracture risk and discussed in more detail in this chapter at Section5.7.

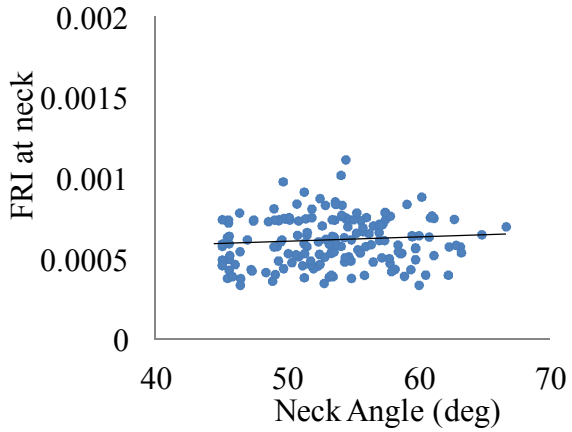

(a)

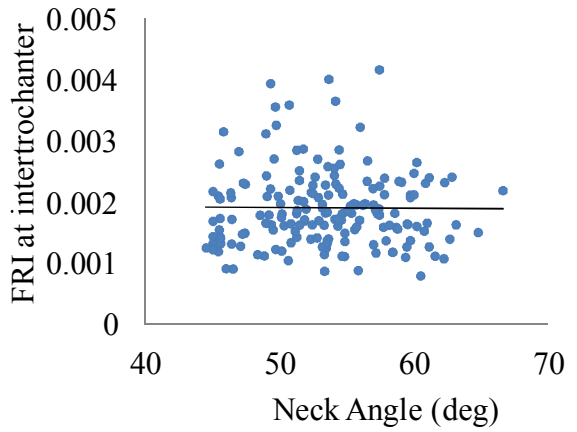

(b)

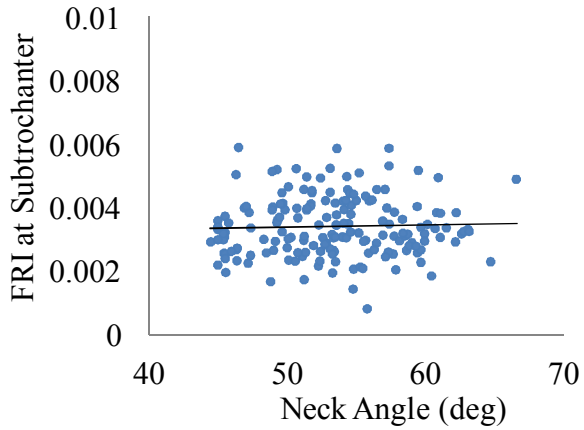

(c)

Figure 5-16: Finite element-computed FRI for fall on greater trochanter versus neck angle of the femur at three critical sections (a) femoral neck (b) intertrochanter and (c) subtrochanter

The correlation coefficients between weight and geometric factors with FRI were calculated using MATLAB "corrcoef" function. The calculated results are given in the following table:

Table 3: Correlation coefficients at three sections

Sections	Correlation coefficients (r) with Fracture risk index and different factors (p-value)					
	Density	Applied load (Body weight)	Total Length	Neck length	Neck Diameter	Neck Angle
Femoral Neck	-0.3274 (>0.001)	0.5164 (>0.001)	0.1330 (0.1062)	0.1077 (0.1175)	0.1618 (0.0267)	0.0866 (0.2637)
Intertro-chanter	-0.6715 (>0.001)	0.1797 (0.017)	0.1967 (0.01)	0.2027 (0.009)	0.3346 (>0.001)	0.00316 (0.9676)
Subtro-chanter	-0.4323 (>0.001)	0.5654 (>0.001)	0.2871 (0.0009)	0.3192 (>0.001)	0.2825 (0.0002)	0.0316 (0.6759)

5.4 Factors Affecting Finite Element Accuracy

The factors mainly affecting the finite element results are geometry, material property and applied boundary conditions. Mesh size may also be considered as an important factor affecting the geometry. The finite element results vary in a response to mesh size. A mesh convergence test was performed to show the effect of the mesh sizes, and it was found that the FRI converges to a steady value for a fine mesh (Figure 5-4). The boundary conditions and load application procedure remained constant for all the cases, with the only change being in the magnitude of loading. Since a subject-specific finite element model was generated, individuals' body weight was used as the load for each case. Similar to the mesh size, the width of the region used for the computation of fracture risk in-

dex is also affected by the geometry as well as material property. In order to demonstrate these affects, a convergence test for the region width was also carried out (Figure 5-6) and FRI declined slightly with the decrease of width.

In this study, the femur head was separated from the hip by selecting three points on the femur head. Though process required manual interactions the error in FRI is insignificant.

5.5 Influence of BMD on FRI

A strong negative correlation between finite element results (FRI) and density can be observed from Figure 5-10 (a, b, c). It can be seen that fracture risk is strongly related to bone density at the intertrochanteric section (r = -0.6715, p<0.001) than at the femoral neck (r = -0.3274, p<0.001) or subtrochanteric region (r = -0.4323, p<0.001). These results are in good agreement with Lang *et al*. [75] and Cheng *et al*. [108]. Lang *et al.* [75] found that femur strength is strongly dependent (R^2 = 87%) on trochanteric BMD which indicates that trochanteric density is mostly responsible for trochanteric fracture. In addition, higher BMD leads to increased femur strength with a decrease in fracture risk and vice versa.

5.6 Influence of Patient's Body Weight on FRI

Fracture risk is strongly correlated with body weight but the magnitude of correlation varies from location to location. A weak positive correlation between fracture risk and

body weight (r = 0.1797, p=0.017) was observed at the intertrochanteric section (Figure 5-11 (b)). On the other hand, femoral neck FRI (r = 0.5164, p<0.001) and subtrochanteric FRI (r = 0.5654, p<0.001) more dependent on body weight than density (Figure 5-11). Since body weight was considered as the applied load on the femur, and since the distribution of actual stress depends on the load, an increment in body weight increases the actual stress. As a result, fracture risk increased with greater weight according to the definition of FRI despite higher BMD.

5.7 Influence of Hip Geometric Parameters on FRI

The effects of geometric parameters on FRI were also investigated in this study along with density and fracture load. If the geometry of the hip affects fracture risk, geometric measurements might be used together with densitometric measurements for assessing fracture risk. A better assessment of hip fracture risk might then be obtained from a combined approach rather than from density measurement alone. The total length of the femur, neck length, neck diameter and neck angle are the main geometric parameters investigated in the current study. All these factors were calculated from the source images. The fracture risk index was compared individually for these geometric parameters with the FRI.

Total length of the femur is defined as the distance between the top most point of the femur to the bottom most point of image finite element mesh. The correlations between

FRI and total length at the sections were calculated and scatter plots shown in Figure 5-12. A weak positive correlation was found between these two factors. The results are in good agreement with a population based cohort study indicating that taller people are at higher risk of fracture than shorter people [113] (as taller people have longer femur length). Among the three sections studied here, the correlation is strongest for subtrochanteric section (r = 0.2871, p=0.0009) than neck (r = 0.1330, p=0.1062) followed by intertrochanter (r = 0.1939, p=0.01).

Neck length (NL) (defined in Chapter 4) is sometimes referred as HAL (Hip Axis length) and is a weaker predictor of fracture than hip BMD. This factor has an effect on fracture risk but the magnitude varies from weak to strong. It has been stated that, the impact stress of the proximal femur caused by a fall is positively correlated with longer femoral neck length [114]. In contrast, some researchers find that femoral neck length does not necessarily affect fracture risk [115, 116]. In this study, a weak positive correlation was observed between FRI and neck length at the three sections. Like the total length, neck length correlates with FRI at the subtrochanteric section slightly more (r = 0.3192, p<0.001) than the other sections (neck, r = 0.1054, p=0.1175 and intertrochanter, r = 0.1942, p=0.009). It is still unknown how the NL influenced the fracture at subtrochanter in a larger scale. Several possible explanations have been proposed, including the concept of NL coinciding with the femoral moment arm [114, 117] and may also be a measure of the degree to which the femur extends beyond the pelvis, increasing risk for impact [118]. Because of the lack of definitive evidence regarding HAL or NL, it is not recommended for clinical use alone; rather, should only be used in conjunction with BMD and considered as an auxiliary risk factor.

FRI is positively correlated with neck diameter at the femoral neck (r = 0.1618, p<0.0267), the intertrochanter (r = 0.3346, p<0.001) and the subtrochanter (r = 0.2825, p=0.0002). This behavior is not consistent with beam theory. In general, greater diameters should improve fracture resistance and thus reduce fracture risk. An unexpected observation borne out in several other studies is that hip fracture cases had wider femoral neck [119, 120, 121]. One possible explanation is that as diameter is increased, locally thin sections of cortex are prone to becoming unstable under compressive loading [85]. Alternatively, femoral neck diameter is strongly dependent on femoral neck length (r = 0.8714, p<0.001) and a larger neck length generally increases the fracture risk.

Neck angle does not show any observable correlation with FRI at the sections except for femoral neck (see Figure 5-16). At the femoral neck, a positive (r = 0.0866, p=0.2637) but very weak correlation was found. At the intertrochanter and subtrochanteric section no correlation between FRI and neck angle was observed which is similar to the study of Faulkner *et al*. [122]. They found no significant correlation between neck-shaft angle and hip fracture risk.

As the geometrical parameters of femur are internally related to each other, a single parameter is inadequate to evaluate the exact relation with fracture risk. The combination of geometric parameters can better explain the relationship with the FRI.

5.8 Multivariable Regression Analysis

Osteoporotic fracture risk depends not only on BMD but may also be affected by other factors like body weight, femoral neck length, narrowest neck diameter, neck angle or total length. The combined effects of all of these parameters may more accurately determine the fracture risk index. A multiple linear regression analysis was performed for all 180 cases. In this analysis, body weight, bone density, total femur length, neck length, neck diameter and neck angle were used as independent variables and FE computed FRI was considered as the dependent variable. The calculation was performed at three sections (i.e. at femoral neck, intertrochanter and subtrochanter).

Table 4: Results for multiple regression at femoral neck

Regression Statistics	
Multiple R	0.594174294
R Square	0.353043092
Adjusted R Square	0.328782208
Standard Error	0.00012261
Observations	180

	Coefficients	Standard Error	*t* Stat	*P*-value
Intercept	0.000455847	0.000167658	2.718913	0.007272792
BMD	-1.27705E-06	3.48124E-07	-3.66838	0.000331952
Body weight	2.60624E-06	3.27014E-07	7.969805	2.82182E-13
Total length	3.14456E-06	1.54017E-06	2.041698	0.042823879
Neck Length	-6.6816E-06	2.87008E-06	-2.32802	0.021163095
Neck diameter	7.15801E-06	6.8281E-06	1.048318	0.296073172
Neck Angle	3.77705E-06	2.07456E-06	1.82065	0.070528535

Table 5: Results for multiple regression at intertrochanter

Regression Statistics	
Multiple R	0.80903615
R Square	0.654539492
Adjusted R Square	0.642201616
Standard Error	0.000373248
Observations	180

	Coefficients	Standard Error	*t* Stat	*P*-value
Intercept	0.004144428	0.000480051	8.633306	4.40911E-15
BMD	-1.30611E-05	8.45824E-07	-15.4419	4.69797E-34
Body weight	9.64867E-06	1.05063E-06	9.183703	1.5162E-16
Total length	2.32248E-06	4.5999E-06	0.504898	0.614291802
Neck length	6.15481E-06	8.76747E-06	0.702006	0.483647143
Neck diameter	-1.92981E-05	2.18518E-05	-0.88313	0.378425606
Neck Angle	8.75344E-06	5.98938E-06	1.461493	0.145748201

Table 6: Results for multiple regression at subtrochanter

Regression Statistics	
Multiple R	0.681516693
R Square	0.464465003
Adjusted R Square	0.445338753
Standard Error	0.000692835
Observations	180

	Coefficients	Standard Error	*t* Stat	*P*-value
Intercept	0.003651517	0.001004898	3.633719653	0.000370937
BMD	-6.93894E-06	1.19752E-06	-5.794411782	3.3048E-08
Body weight	1.9348E-05	1.88769E-06	10.24957768	1.8758E-19
Total length	6.5629E-06	8.54841E-06	0.767733227	0.443723398
Neck length	1.217E-05	1.56987E-05	0.775223144	0.439297623
Neck diameter	-4.07315E-05	3.63927E-05	-1.119223302	0.264642547
Neck angle	-8.02391E-07	1.10933E-05	-0.072330916	0.942424602

The multiple R between predicted FRI and FE computed FRI were 59.42%, 80.9% and 68.15% at femoral neck, intertrochanter and subtrochanter respectively. FRI is affected significantly by both BMD and body weight at all the three sections. It is also evident from the results presented in Table 4, 5 and 6 that neck angle has negligible effect on the FRI. The results obtained using multiple regression generally agree with the results if the effects of the factors are considered individually.

Chapter 6

Conclusions and Future Work

In the research conducted, a framework for 2D finite element analysis of proximal femur from DXA images was developed. The construction begins with data extraction from DXA images followed by manual intervention for separating the femur from the pelvis, grouping the DXA images, selecting specific points for identifying the femoral neck, the intertrochanter and the subtrochanteric regions. Finally, the developed code was validated and used to generate the FEMs for the 180 cases.

Contributions of the current research:

The major conclusions of the current study can be stated as follows:

- The current FE model used the grey-scale values from the DXA images to map the inhomogeneous material properties of bone. As a result, this FE model was capable of representing the heterogeneous distribution of the material properties of specific femur. Moreover, patient body weight was also incorporated in the model to inform the loading condition instead of using a constant value.

- It was found that osteoporotic fracture risk is not only a function of BMD, but also other factors like body weight and geometric parameters such as femur length, neck length, neck diameter, etc. The effect of these factors varies with the location of the femur. Density has a larger effect on the fracture risk index at the intertrochanteric section. In contrast, body weight exerts greater effect on osteoporotic fracture risk at the femoral neck and subtrochanteric sections. The geometric parameters are made a larger contribution to fracture risk at these two sections than at the intertrochanteric section.
- Although CT (Computed Tomography) based 3D analysis can give reliable anatomic information on the complex proximal femur, a 2D finite element model from X-ray images may be sufficient for clinical purposes [96]. DXA scanners are widely available, and play a primary role in clinical practice. A 2D FE model is capable of integrating the structural behaviour of the proximal femur with the mineral density information available from the DXA scan. Though it was a drastic simplification, a 2D model of the proximal femur in previous studies produced reasonably accurate results under certain loading configurations [123, 124].
- Two dimensional FEM from DXA images have already been used to determine the fracture risk and to predict vertebral fractures [125]. A 2D finite element analysis of fall-related hip fracture is acceptable as falling results in stress and strain lying predominantly in the frontal plane. Results from 2D finite element analyses have been previously validated with those obtained with a 3D finite element analysis of CT data. Testi *et al*. [101] found good agreement between the re-

sults of a 2D finite element model with a DXA image to 3D finite element model, and also validated the results *in-vitro*. Comparing with the aBMD, significance level of 2D finite element analysis from X-ray image is higher than 3D FE analysis [96].

Limitations of the current study:

Even if a relatively good correlation between fracture risk and the various factors has been found from this 2D-DXA based FE model and in agreement with previous research, some limitations of the current study have been identified. In the next paragraphs the limitations of this study and the way to minimize these limitations are discussed.

- It is well-known that the accuracy of any simulation depends on proper modeling of the problem. The risk of femoral fracture not only depends on bone 'quality', but also on a patient's risk for falling, weight, height, proprioception and coordination, skeletal anatomy and anthropometry. Low bone mass as measured by DXA is a major risk factor, but other factors can provide information on fracture risk that is independent of BMD. These include age, low body mass index, previous fracture, family history of hip fracture, glucocorticoid therapy, alcohol abuse, tobacco use and rheumatoid arthritis. Although patient weight and skeletal anatomy were considered along with the bone density in this research, the addition of these other factors may increase the accuracy of the finite element results.
- A limitation of this study is that the femur head separation method was not automated. The process of separating the femur head required manual intervention, which contributed a small amount of error in the FRI calculation.

- The code for extracting the boundary or edge detection from the image was only developed for the left femur, and therefore, it was necessary to invert images of the right femur. The separation procedure was not automated and the user had to manually identify before perform the step edge detection. This was feasible for a smaller number of samples, but would be difficult and time consuming for a large number of samples.
- In this study a uniform distribution of loading on the femur head and greater trochanter was considered. Future work should consider alternative load distributions. Moreover, the direction of fall and the energy absorbed during impact are important issues that deserve further consideration. In the reported research, the direction of loading was not investigated though it may affect the fracture risk index. Due to the limitations of 2D data, the rotational angle had to be ignored. It has been shown in a previous study [126] that a slight variation in loading angle can affect the fracture load due to differences in structural capacity of the femur depending on the fall orientation.
- In the present study, a linear correlation was assumed between pixel value and density. Unfortunately, the density calculated from the image and the BMD values obtained with the images did not show very strong correlation. This might happen due to the nonlinearity in converting the DXA images to JPEG format.

Future Work:

Osteoporosis is the most important condition causing hip fractures. Patients with osteoporosis are at greater risk for developing a hip fracture from accidents such as fall because

of thinner and weaker bones. The risk of hip fracture in older individuals is increasing at the similar rate with the life expectancy. So, there is an urgent need for a more accurate tool in the assessment of osteoporotic fracture risk. An advanced finite element study was proposed here to assess osteoporotic fracture risk and investigate the factors affecting the risk. The minimization of these limitations discussed in the previous section can be considered in possible future work.

- The manual femur head separation process contributed a small amount of error in the FRI and an automated, consistent method for femur head isolation could be beneficial.
- Although FE results were not affected by the inversion operation for analysing the images of right femur, process could be simplified by incorporating a technique for automatic recognition of left femur or right femur.
- The direction and distribution of body weight would be an area of further investigation in future study.
- Finding out the proper relationship between the grey-scale intensity of the DXA image and the JPEG image is an important area of future work to ensure consistency between the FE and clinical results.
- It is evident from the results that BMD alone is not enough for assessing osteoporotic fracture risk. Geometric parameters and body weight need to be considered. The combined effect of all these parameters needs to be clinically tested for the prospective assessment of osteoporotic fractures.

- The processes used in this research might also be useful for longitudinal monitoring of osteoporotic fracture risk. Follow up images may include alterations in in positioning or other technical factors, such as rotation. In addition, the total length of the image may change from the base line images. A method should be introduced to minimize these technical differences between the base line image and follow up image before analysis.

There is a growing awareness that treatment of osteoporosis should be targeted on the basis of fracture risk rather than solely on the information provided by a BMD test. This study focused on fracture risk using BMD information and also geometric information from DXA images in osteoporotic patients. In this study, falling was considered for the evaluation of osteoporotic fracture risk as this is the strongest single risk factor for fractures in elderly people. The sensitivity of the study can be increased for further and future studies by addressing the limitations of this present study. In conclusion, this finite element study using DXA images provides a well-organized, less time consuming tool for fracture type prediction applicable at lower cost and with a smaller radiation dose compare to CT based finite element model.

Bibliography

[1] U. Bergstrom, U. Bjornstig, H. Stenlund, H. Jonsson, and O. Svensson, "Fracture mechanisms and fracture pattern in men and women aged 50 years and older: A study of a 12-year population-based injury register, Umea, Sweden," *Osteoporosis International*, vol. 19, pp. 1267–1273, 2008.

[2] J. Stevens, K. Mack, L. Paulozzi, and M. Ballesteros, "Self-reported falls and fall-related injuries among persons aged 65 years>= United States, 2006," *Journal of Safety Research*, vol. 39, pp. 345–349, 2008.

[3] M. Wiktorowicz and R. Goeree, "Economic implications of hip fracture: health service use, institutional care and cost in Canada," *Osteoporosis International*, vol. 12, pp. 271–278, 2001.

[4] G. S. Keene, M. J. Parker, and G. A. Pryor, "Mortality and morbidity after hip fractures," *British Medical Journal*, vol. 307, pp. 1248–1250, 1993.

[5] [Online]. Available: http://www.nof.org/.

[6] R. Burge, B. Dawson-Hughes, D. H. Solomon, J. B. Wong, A. King, and A. Tosteson, "Incidence and economic burden of osteoporosis-related fractures in the United States, 2005-2025," *Journal of Bone and Mineral Research*, vol. 22, pp. 465–475, 2007.

[7] J. S. Bauer, S. Kohlmann, F. Eckstein, D. Mueller, E.-M. Lochmuller, and T. M. Link, "Structural analysis of trabecular bone of the proximal femur using multislice computed tomography: A comparison with dual x-ray absorptiometry for predicting biomechanical strength in vitro," *Calcified Tissue International*, vol. 78, pp. 78–89, 2006.

[8] D. Marshall, O. Johnell, and H. Wedel, "Meta-analysis of how well measures of bone mineral density predict occurrence of osteoporotic fractures." *British Medical Journal*, vol. 312, pp. 1254–1259, 1996.

[9] [Online]. Available: http://www.radiologyinfo.org/en/info.cfm?pg=dexa

[10] S. A. Wainwright, L. M. Marshall, K. E. Ensrud, J. A. Cauley, D. M. Black, T. A. Hillier, M. C. Hochberg, M. T. Vogt, , and E. S. Orwoll, "Hip fracture in women without osteoporosis," *The Journal of clinical Endocrinology and Metabolism*, vol. 90, pp. 2787–2793, 2005.

[11] T. J. Beck, A. C. Looker, C. B. Ruff, H. Sievanen, and H. w. Wahner, "Structural trends in the aging femoral neck and proximal shaft: Analysis of the Third National Health and Nutrition Examination Survey Dual-Energy X-Ray Absorptiometry data," *Journal of Bone and Mineral Research*, vol. 15, pp. 2297–2304, 2000.

[12] T. J. Beck, C. B. Ruff, K. E. Warden, W. W. Scott, and G. U. Rao, "Predicting femoral neck strength from bone mineral data. A structural approach," *Investigative Radiology*, vol. 25, p. 6, 1990.

[13] S. P. Nielsen, "The fallacy of BMD: A critical review of diagnostic use of DXA," *Clinical Rheumatology*, vol. 19, pp. 174–183, 2000.

[14] B. R. McCreadie and S. A. Goldstein, “Biomechanics of bone fracture: Is bone mineral density sufficient to assess risk?” *Journal of Bone and Mineral Research*, vol. 15, pp. 2305–2308, 2000.

[15] W. C. Hayes, E. R. Myers, S. N. Robinovitch, A. V. D. Kroonenberg, A. C. Courtney, and T. A. McMahon, “Etiology and prevention of age related bone fracture,” *Bone*, vol. 18, p. 1, 1996.

[16] D. Christen, D. J. Webster, and R. Muller, “Multi scale modeling and non linear finite element analysis as clinical tools for the assessment of fracture risk,” *PhilosophicalTransactions of the Royal Society A: Mathematical, Physical and Engineering Sciences*, vol. 368, pp. 2653–2668, 2010.

[17] L. Lenaerts and G. H. van Lenthe, “Multi-level patient-specific modelling of the proximal femur. A promising tool to quantify the effect of osteoporosis treatment,” *PhilosophicalTransactions of the Royal Society A: Mathematical, Physical and Engineering Sciences*, vol. 367, pp. 2079–2093, 2009.

[18] W. Leslie, P. Pahlavan, J. F. Tsang, L. M. Lix, and for the Manitoba Bone Density Program, “Prediction of hip and other osteoporotic fractures from hip geometry in a large clinical cohort,” *Osteoporosis International*, vol. 20, pp. 1767–1774, 2009.

[19] J. H. Keyak, T. S. Kaneko, J. Tehranzadeh, and H. B. Skinner, “Predicting proximal femoral strength using structural engineering models,” *Clinical Orthopaedics and Related Research*, vol. 437, pp. 219–228, 2005.

[20] L. Yang, N. Peel, J. A. Clowes, E. V. McCloskey, and R. Eastell, “Use of DXA-based structural engineering models of the proximal femur to discriminate hip fracture,” *Journal of Bone and Mineral research*, vol. 24, pp. 33–42, 2009.

[21] T. Ruberg, "Computer simulation of adaptive bone remodeling," Ph.D. dissertation, Technische Universitat Braunschweig, Germany, 2004.

[22] [Online]. Available: http://www.augustatech.edu/anatomy/chapter%206.html

[23] R. Ruimerman, "Modeling and remodeling in bone tissue," Ph.D. dissertation, Technische Universiteit Eindhoven, 2005.

[24] L. F. Bonewald, "Osteocytes as dynamic multifunctional cells," *Annals of the New York Academy of Sciences*, vol. 1116, pp. 281–290, 2007.

[25] A. J. Vander, J. H. Sherman, and D. S. Luciano, *Human Physiology*. McGraw-Hill inc, New York, 1994.

[26] [Online]. Available: http://courses.washington.edu/conj/bess/bone/bone2.html

[27] T. Pandorf, A. Haddi, D. C. Wirtz, J. Lammerding, R. Forst, and D. Weichert, "Numerical simulation of adaptive bone remodeling," *Journal of Theoretical and Applied Mechanics*, vol. 37, pp. 639–658, 1999.

[28] D. H. Weinans, R. Huiskes, B. V. Rietbergen, D. R. Sumner, T. M. Turner, and J. O. Galante, "Adaptive bone remodelling around bonded noncemented total hip arthroplasty: A comparison between animal experiments and computer simulation," *Journal of Orthopaedic Research*, vol. 11, pp. 500–513, 1993.

[29] R. Huiskes, R. Ruimerman, G. H. van Lenthe, and J. D. Janssen, "Effects of mechanical forces on maintenance and adaptation of form in trabecular bone," *Nature*, vol. 405, pp. 704–706, 2000.

[30] [Online]. Available: http://media.wiley.com/product_data/excerpt/70/04700196/-0470019670.pdf

[31] W. Xu and K. Robinson, "X-ray image review of the bone remodeling around an osseointegrated trans-femoral implant and a Finite Element simulation case study," *Annals of Biomedical Engineering*, vol. 36, pp. 435–443, 2008.

[32] R. Ruimerman, B. V. Rietbergen, P. Hilbers, and R. Huiskes, "The effects of trabecular-bone loading variables on the surface signaling potential for bone remodeling and adaptation," *Annals of Biomedical Engineering*, vol. 33, pp. 71–78, 2005.

[33] W. S. Group, "Assessment of fracture risk and its application to screening for postmenopausal osteoporosis," World Health Organization, Tech. Rep., 1994.

[34] [Online]. Available: http://www.informedhealthonline.org/fact-sheet-preventing-osteoporosis.423.en.html

[35] A. Moroz, M. C. Crane, G. Smith, and D. I. Wimpenny, "Phenomenological model of bone remodeling cycle containing osteocyte regulation loop," *Biosystems*, vol. 84, pp. 183–190, 2006.

[36] T. Daniel, *Metabolic bone disease. Textbook of Primary Care Medicine*, J. N. (ed). St. Louis, Ed. CV Mosby Publisher, 1999.

[37] H. Charles, *Approach to the elderly patient with osteopenia or osteoporosis. Textbook of Internal Medicine.*, W. N. (ed). Philadelphia, Ed. Lippincott-Raven Publishers, 1997.

[38] [Online]. Available: http://www.osteoporosis.ca/index.php/ci_id/8867/la_id/1.htm

[39] J. A. Kanis, "WHO technical report," University of Sheffield, Tech. Rep., 2007.

[40] R. D. Wasnich, "Perspective on fracture risk and phalangeal bone mineral density," *Journal of Clinical Densitometry*, vol. 1, pp. 259–268, 1998.

[41] P. Pietschmann, M. Rauner, and W. Sipos, "Osteoporosis: An age-related and gender-specific disease - A mini-review," *Gerontology*, vol. 55, pp. 3–12, 2008.

[42] W. D. Leslie, S. O. Donnell, C. Lagace, P. Walsh, C. Bancej, S. Jean, K. Siminoski, S. Kaiser, D. L. Kendler, and S. Jaglal, "Population based Canadian hip fracture rates with international comparison," *Osteoporosis International*, vol. 21, pp. 1317–1322, 2010.

[43] E. J. Samelson and M. T. Hannan, "Epidemiology of osteoporosis," *Current Rheumatology Reports*, vol. 8, pp. 76–83, 2006.

[44] B. Riggs and L. M. III, "The world wide problem of osteoporosis: Insights afforded by epidemiology," *Bone*, vol. 17, pp. S505–S511, 1995.

[45] B. Borah, G. J. Gross, T. E. Dufresne, T. S. Smith, M. D. Cockman, P. A. Chmielewski, M. W. Lundy, J. R. Hartke, and E. W. Sod, "Three dimensional micro imaging, finite element modeling and rapid prototyping provide unique insights into bone architecture in osteoporosis," *The Anatomical Record*, vol. 265, pp. 101–110, 2001.

[46] J. Davis, M. Robertson, M. Ashe, T. Liu-Ambrose, K. Khan, and C. Marra, "International comparison of cost of falls in older adults living in the community: A systematic review," *Osteoporosis International*, vol. 21, p. 1295, 2010.

[47] [Online]. Available: www.cdc.gov/ncipc/wisqars

[48] R. Y. Hinton, D. W. Lennox, F. R. Ebert, S. J. Jacobsen, and G. G. Smith, "Relative rates of fracture of the hip in the United States geographic, sex, and age variations," *Journal of Bone and Joint Surgery*, vol. 77, pp. 695–702, 1995.

[49] [Online]. Available: http://advancedortho.net/info/hipfractureinfo.php

[50] O. Lofman, K. Berglund, L. Larsson, and G. Toss, "Changes in hip fracture epidemiology: Redistribution between ages, genders and fracture types," *Osteoporosis International*, vol. 13, pp. 18–25, 2002.

[51] M. R. Karagas, G. L. Lu-Yao, J. A. Barrett, M. L. Beach, and J. A. Baron, "Heterogeneity of hip fracture: Age, race, sex, and geographic patterns of femoral neck and trochanteric fractures among the US elderly," *American Journal of Epidemiology*, vol. 143, pp. 677–682, 1996.

[52] R. Hinton and G. Smith, "The association of age, race, and sex with the location of proximal femoral fractures in the elderly," *Journal of Bone and Joint Surgery*, vol. 75, pp. 752–759, 1993.

[53] J. D. Michelson, A. Myers, R. Jinnah, Q. Cox, and M. V. Natta, "Epidemiology of hip fractures among the elderly: Risk factors for fracture type," *Clinical Orthopaedics and Related Research*, vol. 311, pp. 129–135, 1995.

[54] E. Barrett-Connor, E. S. Siris, L. E. Wehren, P. D. Miller, T. A. Abbott, M. L. Berger, A. C. Santora, and L. M. Sherwood, "Osteoporosis and fracture risk in women of different ethnic groups," *Journal of bone and mineral research*, vol. 20, pp. 185–194, 2005.

[55] P. D. Ross, H. Norimatsu, J. W. Davis, K. Yano, R. D. Wasnich, S. Fujiwara, Y. Hosoda, and L. J. Melton, "A comparison of hip fracture incidence among native Japanese, Japanese Americans, and American Caucasians," *American Journal of Epidemiology*, vol. 133, pp. 801–809, 1991.

[56] P. D. Ross, Y.-F. He, A. J. Yates, C. Coupland, P. Ravn, M. McClung, D. Thompson, and R. D. Wasnich, "Body size accounts for most differences in bone den-

sity between Asian and Caucasian women," *Calcified Tissue International*, vol. 59, pp. 339–343, 1996.

[57] S. R. Cummings, J. A. Cauley, L. Palermo, P. D. Ross, R. D. Wasnich, D. Black, and K. G. Faulkner, "Racial differences in hip axis lengths might explain racial differences in rates of hip fracture," *Osteoporosis International*, vol. 4, pp. 226–229, 1994.

[58] [Online]. Available: www.mdguidelines.com

[59] S. C. Gallannaugh, A. Martin, and P. Millard, "Regional survey of femoral neck fractures," *British medical journal*, vol. 2, pp. 1496–1497, 1976.

[60] A. Fisher, M. Davis, S. Rubenach, D. L. Couteur, and A. McLean, "The site-specific epidemiology of hip fracture in the Australian capital territory with pojections for the first half of the 21st century: Implications for clinical management and health services planning," *Australasian Journal on Ageing*, vol. 26, pp. 45–51, 2007.

[61] C. H. Orces, "Epidemiology of hip fractures in Ecuador," *Revista Panamericana de Salud Publica*, vol. 25, pp. 438–442, 2009.

[62] H. Hagino, T. Nakamura, K. Sakamoto, K. Yamamoto, N. Endo, S. Mori, Y. Mutoh, S. Yamamoto, A. Harada, and K. Kushida, "Nationwide survey of hip fractures in Japan. Committee for Osteoporosis Treatment of The Japanese Orthopaedic Association," *Journal of Orthopaedic Science*, vol. 9, pp. 1–5, 2004.

[63] T. David, K. Marita, C. Richard, C. Bert, and G. Jason, "Hip fracture types in men and women change differently with age," *BMC Geriatrics*, vol. 10, p. 12, 2010.

[64] [Online]. Available: http://emedicine.medscape.com/article/393602-overview#a01

[65] [Online]. Available: http://www.nevdgp.org.au/info/ArthritisF/arthritis/bone.htm

[66] "A practical guide to bone densitometry in children," national Osteoporosis Society, Camerton, Bath, UK.

[67] L. A. Binkovitz and M. J. Henwood, "Pediatric DXA: technique and interpretation," *Pediatric radiology*, vol. 37, pp. 21–31, 2007.

[68] M. E. Elliott and N. Binkley, "Evaluation and measurement of bone mass," *Epilepsy and Bone Health*, vol. 5, pp. 16–23, 2004.

[69] N. B. Watts, "Fundamentals and pitfalls of bone densitometry using dual-energy x-ray absorptiometry (DXA)," *Osteoporosis International*, vol. 15, pp. 847–854, 2004.

[70] [Online]. Available: http://www.capitalimagingassoc.com/dxa.html

[71] G. M. Kiebzak, K. G. Faulkner, W. Wacker, R. Hamdy, E. Seier, and N. B. Watts, "Effect of precision error on T-scores and the diagnostic classification of bone status," *Journal of Clinical Densitometry*, vol. 10, pp. 239–243, 2007.

[72] J. Bauer, S. Virmani, and D. Mueller, "Quantitative CT to assess bone mineral density as a diagnostic tool for osteoporosis and related fractures," *Clinical applications Investigations and research*. [Online]. Available: http://incenter.medical.philips.com/-doclib/enc/fetch/2000/4504/577242/577256/588821/5050628/5313460/6788482/-MM_54-2_INT_07_Bauer.pdf%3fnodeid%3d6789799%26vernum%3d1

[73] S. Cummings, W. Browner, S. Cummings, D. Black, M. Nevitt, W. Browner, H. Genant, J. Cauley, K. Ensrud, J. Scott, and T. Vogt, "Bone density at various sites for prediction hip fracture," *Lancet*, vol. 341, pp. 72–75, 1993.

[74] A. M. Schott, C. Cormier, D. Hans, F. Favier, E. Hausherr, P. Dargent-Molina, P. D. Delmas, C. Ribot, J. L. Sebert, G. Breart, and P. J. M. et.al, "How hip and whole-

body bone mineral density predict hip fracture in elderly women: The EPIDOS prospective study," *Osteoporosis International*, vol. 8, pp. 247–254, 1998.

[75] T. Lang, J. Keyak, M. Heitz, P. Augat, Y. Lu, A. Mathur, and H. Genant, "Volumetric quantitative computed tomography of the proximal femur: precision and relation to bone strength," *Bone*, vol. 21, pp. 101–108, 1997.

[76] T. F. Lang, J. Li, S. T. Harris, and H. K. Genant, "Assessment of vertebral bone mineral density using volumetric quantitative CT," *Journal of Computer Assisted Tomography*, vol. 23, pp. 130–137, 1999.

[77] J. H. Keyak, S. A. Rossi, K. A. Jones, and H. B. Skinner, "Prediction of femoral fracture load using automated Finite Element Modeling," *Journal of Biomechanics*, vol. 31, pp. 125–133, 1997.

[78] N. J. Crabtree, H. Kroger, A. Martin, H. A. P. Pols, R. Lorenc, J. Nijs, J. J. Stepan, J. A. Falch, T. Miazgowski, S. Grazio, P. Raptou, J. Adams, A. Collings, K.-T. Khaw, N. Rushton, M. Lunt, A. K. Dixon, and J. Reeve, "Improving risk assessment: Hip geometry, bone mineral distribution and bone strength in hip fracture cases and controls. The EPOS Study," *Osteoporosis International*, vol. 13, pp. 48–54, 2002.

[79] N. Crabtree, M. Lunt, G. Holt, H. Kroger, H. Burger, S. Grazio, K.-T. Khaw, R. Lorenc, J. Nijs, J. Stepan, J. Falch, T. Miazgowski, P. Raptou, H. Pols, J. Dequeker, S. Havelka, K. Hoszowski, I. Jajic, S. Czekalski, G. Lyritis, A. Silman, and J. Reeve, "Hip geometry, bone mineral distribution, and bone strength in European men and women: The EPOS study," *Bone*, vol. 27, pp. 151–159, 2000.

[80] T. J. Beck, C. B. Ruff, W. W. Scott, C. C. Plato, J. D. Tobin, and C. A. Quan, "Sex differences in geometry of the femoral neck with aging: A structural analysis of bone mineral data," *Calcified Tissue International*, vol. 50, pp. 24–29, 1992.

[81] T. J. Beck, C. B. Ruff, and K. Bissessur, "Age-related changes in female femoral neck geometry: Implications for bone strength," *Calcified tissue international*, vol. 53, pp. S41–S46, 1993.

[82] K. Uusi-Rasi, T. J. Beck, L. M. Semanick, M. M. Daphtary, G. G. Crans, D. Desaiah, and K. D. Harper, "Structural effects of raloxifene on the proximal femur: results from the multiple outcomes of raloxifene evaluation trial," *Osteoporosis International*, vol. 17, pp. 575–586, 2006.

[83] J. Takada, G. Katahira, K. Iba, T. Yoshizaki, and T. Yamashita, "Hip structure analysis of bisphosphonate-treated japanese postmenopausal women with osteoporosis," *Journal of Bone Mineral Metabolism*, vol. 29, pp. 458–465, 2011.

[84] T. J. Beck, "Extending DXA beyond bone mineral density: Understanding hip structure analysis," *Current Osteoporosis Reports*, vol. 5, pp. 49–55, 2007.

[85] S. Kaptoge, T. J. Beck, J. Reeve, K. L. Stone, T. A. Hillier, J. A. Cauley, and S. R. Cummings, "Prediction of incident hip fracture risk by femur geometry variables measured by hip structural analysis in the study of osteoporotic fractures," *Journal of Bone and Mineral Research*, vol. 23, pp. 1892–1904, 2008.

[86] B. C. C. Khoo, T. J. Beck, Q.-H. Qiao, P. Parakh, L. Semanick, R. L. Prince, K. P. Singer, and R. I. Price, "In vivo short-term reproducibility of hip structure analysis variables in comparison with bone mineral density using paired dual-energy x-ray absorptiometry scans from multi-centre clinical trials," *Bone*, vol. 37, pp. 112–121, 2005.

[87] J. A. Kanis, H. Johansson, A. Oden, and E. V. McCloske, "Assessment of fracture risk," *European Journal of Radiology*, vol. 71, pp. 392–397, 2009.

[88] J. A. Kanis, O. Johnell, A. Oden, H. Johansson, and E. McCloskey, "FRAX and the assessment of fracture probability in men and women from the UK," *Osteoporosis International*, vol. 19, pp. 385–397, 2008.

[89] N. C. Wright and K. G. Saag, "From fracture risk prediction to evaluating fracture patterns: Recent advances in the epidemiology of osteoporosis," *Current Rheumatology report*, vol. 14, pp. 205–211, 2012.

[90] W. D. Leslie, L. M. Lix, H. Johansson, A. Oden, E. McCloskey, and J. A. K. for the Manitoba Bone Density Program, "Independent clinical validation of a canadian FRAX tool: Fracture prediction and model calibration," *Journal of Bone and Mineral Research*, vol. 25, pp. 2350–2358, 2010.

[91] S. Kaptoge, L. Benevolenskaya, A. Bhalla, J. Cannata, S. Boonen, J. Falch, D. Felsenberg, J. Finn, R. Nuti, K. Hoszowski, R. Lorenc, T. Miazgowski, I. Jajic, G. Lyritis, P. Masaryk, M. Naves-Diaz, G. Poor, D. Reid, C. Scheidt-Nave, J. Stepan, C. Todd, K. Weber, A. Woolf, D. Roy, M. Lunt, S. Pye, T. O'Neill, A. Silman, and J. Reeve, "Low BMD is less predictive than reported falls for future limb fractures in women across Europe: results from the European Prospective Osteoporosis study," *Bone*, vol. 36, pp. 387–398, 2005.

[92] T. L. N. Järvinen, H. Sievänen, K. M. Khan, A. Heinonen, and P. Kannus, "Shifting the focus in fracture prevention from osteoporosis to falls," *British Medical Journal*, vol. 336, pp. 124–126, 2008.

[93] E. Madenci and I. Guven, *The finite element method and applications in engineering using ANSYS*. Springer, 2006.

[94] R. Huskies and E. Y. Chao, "A survey of finite element analysis in orthopedic biomechanics: the first decade," *Journal of Biomechanics*, vol. 16, pp. 385–409, 1983.

[95] C. Langtona, S. Pisharody, and J. Keyak, "Comparison of 3d finite element analysis derived stiffness and bmd to determine the failure load of the excised proximal femur," *Medical Engineering & Physics*, vol. 31, pp. 668–672, 2009.

[96] S. Pisharody, R. Phillips, and C. M. Langton, "Sensitivity of proximal femoral stiffness and areal bone mineral density to changes in bone geometry and density," *Proceedings of the Institution of Mechanical Engineers; Part H; Journal of Engineering in Medicine*, vol. 222, pp. 367–375, 2008.

[97] J. O. D. Buijs and D. Dragomir-Daescu, "Validated finite element models of the proximal femur using two-dimensional projected geometry and bone density," *Computer Methods and Programs in Biomedicine*, vol. 104, pp. 168–174, 2010.

[98] J. Thevenot, P. Pulkkinen, J. E. Koivumaki, V. Kuhn, F. Eckstein, and T. Jamsa, "Discrimination of cervical and trochanteric hip fractures using radiography-based two-dimensional finite element models," *The Open Bone Journal*, vol. 1, pp. 16–22, 2009.

[99] D. D. Cody, G. J. Gross, F. J. Hou, H. J. Spencerc, S. A. Goldstein, and D. P. Fyhrie, "Femoral strength is better predicted by finite element models than QCT and DXA," *Journal of Biomechanics*, vol. 32, pp. 1013–1020, 1999.

[100] M. Viceconti, L. Bellingeri, L. Cristofolini, and A. Toni, "A comparative study on different methods of automatic mesh generation of human femurs," *Medical Engineering & Physics*, vol. 20, pp. 1–10, 1998.

[101] D. Testi, M. Viceconti, F. Baruffaldi, and A. Cappello, "Risk of fracture in elderly patients: A new predictive index based on bone mineral density and finite element analysis," *Computer Methods and Programs in Biomedicine*, vol. 60, pp. 23–33, 1999.

[102] D. L. Kopperdahl, E. F. Morgan, and T. M. Keaveny, "Quantitative computed tomography estimates of the mechanical properties of human vertebral trabecular bone," *Journal of Orthopaedic Research*, vol. 20, pp. 801–805, 2002.

[103] D. T. S. Keller, Z. Mao, and D. M. Spengle, "Young's modulus, bending strength, and tissue physical properties of human compact bone," *Journal of Orthopaedic Research*, vol. 8, pp. 592–603, 1990.

[104] C. N. Wu and P. Zhang, "Design of finite element procedure for predicting osteoporotic fractures," Undergraduate thesis, University of Manitoba, 2011.

[105] E. Schileo, E. Dall'Ara, F. Taddei, A. Malandrino, T. Schotkamp, M. Baleani, and M. Viceconti, "An accurate estimation of bone density improves the accuracy of subject-specific finite element models," *Journal of Biomechanics*, vol. 41, pp. 2483–2491, 2008.

[106] B. P. McNamara, L. Cristofolini, A. Toni, and D. Taylor, "Evaluation of experimental and finite element models of synthetic and cadaveric femora for pre-clinical design analysis," *Journal of clinical materials*, vol. 17, pp. 131–140, 1995.

[107] J. A. Cauley, L.-Y. Lui, H. K. Genant, L. Salamone, W. Browner, H. A. Fink, P. Cohen, T. Hillier, D. C. Bauer, and S. R. Cummings, "Risk factors for severity and type of the hip fracture," *Journal of Bone and Mineral Research*, vol. 24, p. 5, 2009.

[108] X. G. Cheng, G. Lowet, S. Boonen, P. H. F. Nicholson, P. Brys, J. Nijs, and J. Dequeker, "Assessment of the strength of proximal femur in vitro: Relationship to femoral bone mineral density and femoral geometry," *Bone*, vol. 20, pp. 213–218, 1997.

[109] J. R. Barber, *Intermediate Mechanics of Materials*. Springer, 2011.

[110] V. D. da Silva, *Mechanics and Strength of Material*. Springer, 2006.

[111] A. Perillo-Marcone, A. Alonso-Vazquez, and M. Taylor, "Assessment of the effect of mesh density on the material property discretization within QCT based FE models: A practical example using the implanted proximal tibia," *Computer Methods in Biomechanics and Biomedical Engineering*, vol. 6, pp. 17–26, 2003.

[112] C.-C. Glüer, G. Blake, Y. Lu, B. A. Blunt, M. Jergas, and H. K. Genant, "Accurate assessment of precision errors: How to measure the reproducibility of bone densitometry techniques," *Osteoporosis International*, vol. 2, pp. 262–270, 1995.

[113] B. Y. Farahmand, K. Michaëlsson, J. A. Baron, P.-G. Persson, and S. Ljunghall, "Body size and hip fracture risk," *Epidemiology*, vol. 11, pp. 214–219, 2000.

[114] H. Ulusoy, A. Bilgici, O. Kuru, N. Sarica, S. Arslan, and U. Erkorkmaz, "A new value of proximal femur geometry to evaluate hip fracture risk: true moment arm," *Hip International*, vol. 18, pp. 101–107, 2008.

[115] J. Panula, M. Savela, P. T. Jaatinen, P. Aarnio, and S.-L. Kivela, "The impact of proximal femur geometry on fracture type: A comparison between cervical and trochanteric fractures with two parameters," *Scandinavian Journal of Surgery*, vol. 97, pp. 266–271, 2008.

[116] J. Michelotti and J. Clark, "Femoral neck length and hip fracture risk," *Journal of Bone and Mineral Research*, vol. 14, pp. 1714–1720, 1999.

[117] M. I. Wani, M. M. Wani, A. Sultan, and T. Dar, "Subtrochanteric fractures- Current management options," *The Internet Journal of Orthopedic Surgery*, vol. 17, p. 2, 2010.

[118] K. Faulkner, "Frequently asked questions regarding hip axis length." [Online]. Available: http://www.gehealthcare.com/gecommunity/lunar/docs/faq_hal.pdf

[119] C.-C. Glüer, S. R. Cummings, A. Pressman, J. Li, K. Glüer, K. G. Faulkner, S. Grampp, and H. K. Genant, "Prediction of hip fractures from pelvic radiographs: The study of osteoporotic fractures. The study of osteoporotic fractures research group," *Journal of Bone and Mineral Research*, vol. 9, pp. 671–677, 1994.

[120] F. Rivadeneira, M. C. Zillikens, C. E. D. Laet, A. Hofman, A. G. Uitterlinden, T. J. Beck, and H. A. Pols, "Femoral neck BMD is a strong predictor of hip fracture susceptibility in elderly men and women because it detects cortical bone instability: The Rotterdam Study," *Journal of Bone and Mineral Research*, vol. 22, pp. 1781–1790, 2007.

[121] S. Gnudi, C. Ripamonti, G. Gualtieri, and N. Malavolta, "Geometry of proximal femur in prediction of hip fracture in osteoporotic women," *British Journal of Radiology*, vol. 72, pp. 729–733, 1999.

[122] K. G. Faulkner, S. R. Cummings, D. Black, L. Palermo, C.-C. Gluer, and H. K. Genant, "Simple measurement of femoral geometry predicts hip fracture: The study of osteoporotic fractures," *Journal of Bone and Mineral Research*, vol. 8, pp. 1211–1217, 1993.

[123] R. Huiskes and W. Vroemen, "A standardized finite element model for routine comparative evaluations of femoral hip prostheses," *Acta Orthopaedica Belgica*, vol. 52, pp. 258–261, 1986.

[124] R. Huiskes, "The various stress patterns of press-fit, ingrown, and cemented femoral stems," *Clinical Orthopaedics and Related Research*, vol. 261, pp. 27–38, 1990.

[125] J. MacNeil, J. Adachi, D. Goltzman, R. Josse, C. Kovacs, J. Prior, W. Olszynski, K. Davison, S. Kaiser, and the CaMos Research Group, "Predicting fracture using 2D finite element modelling," *Medical engineering and physics*, vol. 34, pp. 478–484, 2011.

[126] T. P. Pinilla, K. C. Boardman, M. L. Bouxsein, E. R. Myers, and W. C. Hayes, "Impact direction from a fall influences the failure load of the proximal femur as much as age-related bone loss," *Calcified Tissue International*, vol. 58, pp. 231–235, 1996.